**TITLE**

# Relationships of Alzheimer's disease and apolipoprotein E genotypes with small RNA and protein cargo of brain tissue extracellular vesicles

**AUTHORS**

Yiyao Huang[a,#], Tom A. P. Driedonks[a,#], Lesley Cheng[b], Andrey Turchinovich[c,d], Harinda Rajapaksha[b], Tanina Arab[a], Bonita H. Powell[a], Olga Pletniková[e,f], Javier Redding[e], Juan C. Troncoso[e,g], Laura Vella[h,i], Lei Zheng[j], Andrew F. Hill[b], Vasiliki Mahairaki[f,k], Kenneth W. Witwer[a,f,k,*]

**Affiliations**

[a]Department of Molecular and Comparative Pathobiology, Johns Hopkins University School of Medicine, Baltimore, MD, USA

[b]Department of Biochemistry and Genetics, La Trobe Institute for Molecular Science, La Trobe University, Bundoora, Australia

[c]Molecular Epidemiology, German Cancer Research Center DKFZ, Heidelberg, Germany

[d]SciBerg e.Kfm, Mannheim, Germany

[e]Department of Pathology, Johns Hopkins University School of Medicine, Baltimore, MD, USA

[f]Department of Pathology and Anatomical Sciences, Jacobs School of Medicine and Biomedical Sciences, University at Buffalo, Buffalo, NY, USA

[g]Department of Neurology, Johns Hopkins University School of Medicine, Baltimore, MD, USA

[h]The Florey Institute of Neuroscience and Mental Health, The University of Melbourne, Parkville, Australia

23 [i]Department of Surgery, The University of Melbourne, The Royal Melbourne Hospital, Parkville,
24 Australia
25 [j]Department of Laboratory Medicine, Nanfang Hospital, Southern Medical University,
26 Guangzhou, Guangdong, China
27 [k]Richman Family Precision Medicine Center of Excellence in Alzheimer's Disease, Johns Hopkins
28 University School of Medicine, Baltimore, MD, USA
29
30 [#]These authors contributed equally to this work
31 *Corresponding author
32 Kenneth W. Witwer, kwitwer1@jhmi.edu
33
34 **Email addresses**
35 Yiyao Huang yiyaohuang@jhu.edu
36 Tom A. P. Driedonks tdriedo1@jhu.edu
37 Lesley Cheng l.cheng@latrobe.edu.au
38 Andrey Turchinovich andrey.turchinovich@sciberg.com
39 Harinda Rajapaksha K.Rajapaksha@latrobe.edu.au
40 Tanina Arab tarab1@jhu.edu
41 Bonita H. Powell bpowel15@jhu.edu
42 Olga Pletniková olgaplet@buffalo.edu
43 Javier Redding redding54@jhmi.edu
44 Juan C. Troncoso troncoso@jhmi.edu

45 Laura Vella laura.vella@florey.edu.au

46 Lei Zheng nfyyzhenglei@smu.edu.cn

47 Andrew F. Hill Andrew.Hill@latrobe.edu.au

48 Vasiliki Mahairaki vmachai1@jhmi.edu

49 Kenneth W. Witwer kwitwer1@jhmi.edu

50

**ABSTRACT**

Alzheimer's disease (AD) is a public health crisis that grows as populations age. Hallmarks of this neurodegenerative disease include aggregation of beta-amyloid peptides and hyperphosphorylated tau proteins in the brain. Variants of the APOE gene are the greatest known risk factors for sporadic AD. As emerging players in AD pathophysiology, extracellular vesicles (EVs) contain proteins, lipids, and RNAs and are involved in disposal of cellular toxins and intercellular communication. AD-related changes in the molecular composition of EVs may contribute to pathophysiology and lend insights into disease mechanisms. We recently adapted a method for separation of brain-derived EVs (bdEVs) from post-mortem tissues. Using this method, we isolated bdEVs from AD patients with different APOE genotypes (n=23) and controls (n=7). bdEVs were counted, sized, and subjected to parallel small RNA sequencing and proteomic analysis. Numerous bdEV-associated RNAs and proteins correlated with AD pathology and APOE genotype. Some of the identified entities have been implicated previously in important AD-related pathways, including amyloid processing, neurodegeneration, and metabolic functions. These findings provide further evidence that bdEVs and their molecular cargo modulate development and progression of AD.

**Keywords**

Alzheimer's disease, APOE, brain, extracellular vesicles, exosomes, proteomics, RNA sequencing, neurodegeneration

73 **INTRODUCTION**

74

75 Alzheimer's disease (AD, (1)) is a public health crisis (2,3) that continues to grow as the
76 population ages, demanding new insights into pathophysiology. Mechanisms of pathogenesis
77 are manifold and incompletely understood. Synaptic connections are lost through
78 neurodegeneration. Extracellular deposition of β-amyloid (Aβ—fragments of the amyloid
79 precursor protein, APP) occurs in the form of neuritic plaques (NPs), while intracellular
80 aggregation of hyperphosphorylated tau produces neurofibrillary tangles (NFTs) (4–8). Similar
81 to misfolded prions, pathogenic Aβ and tau can template misfolding and protein modifications
82 at recipient sites (9–11). Wide distribution and high density of NPs and NFTs correspond with
83 greater cognitive impairment. Other hallmarks of AD include vascular amyloidosis, gliosis, and
84 blood-brain barrier disruption (12).

85

86 Numerous genetic risk factors for AD have been identified. Mutations in genes such as
87 presenilin 1 (PSEN1) and APP contribute to early-onset, familial AD (FAD). In sporadic AD,
88 variants of the apolipoprotein E (APOE) gene (*APOE*) are the greatest known genetic risk factor
89 (13–16). A central player in lipid homeostasis, APOE assists in intercellular lipid transfer, binding
90 both cholesterol and low-density lipoprotein receptors in addition to binding Aβ. Three major
91 APOE isoforms exist, encoded by alleles ε2, ε3, and ε4, and produce proteins that differ by only
92 1-2 amino acids but have different binding partner interactions. Whereas APOE2 is protective
93 against AD relative to APOE3, APOE4 is associated with increased risk, particularly in women
94 and certain ethnic populations (17). In Caucasians, the risk of late-onset AD is higher for APOE4

homozygosity (12-fold) and heterozygosity (2-3-fold), with some indication of greater risk for early-onset disease (18). A majority of AD patients in the US have at least one ε4 allele. The critical role of APOE in central nervous system (CNS) lipid metabolism is not limited to AD. The ε4 allele has been associated with increased cholesterol, ceramide, and sphingomyelin in brains of HIV dementia patients (19), a difference not due to inflammation (activated microglia) or astrogliosis. Furthermore, interactions of biological sex (AD disproportionately affects women (20)) and APOE4 have been noted in AD (17,21,22) and AD models (23,24).

Extracellular vesicles (EVs) comprise a diversity of lipid bilayer membrane-delimited particles that dispose cellular toxins and mediate intercellular communication (25–27). Roles for EVs have recently been recognized in AD pathophysiology (28–30). EVs participate in neurodegeneration in AD, Parkinson's, and prion diseases in part by spreading misfolded proteins (31–35). In AD, Aβ and tau have been found in or on EVs in AD models and patients (32–34,36–42). EVs are also found "at the scene of the crime": in amyloid plaques (36,43). EV cargo betray AD and mild cognitive impairment (MCI) (37,39,44–48). Furthermore, some EVs contribute to amyloid clearance by glia (49–51), suggesting that EVs from healthy cells block AD pathology. However, context matters: in certain models, reducing EV release may diminish pathology (52,53). Differential expression of various microRNAs was observed in brain tissue (54–56) and serum of AD patients (57), suggesting that the RNA cargo of EVs may contribute to AD pathogenesis.

116 The study of EVs and APOE, like the study of EVs in AD in general, is just beginning (58–61), but
117 the rapidly growing literature shows that EVs and APOE contribute to AD via multiple
118 mechanisms. At the same time, APOE variants act in lipid homeostasis and trafficking, processes
119 that also govern EV release and uptake. APOE+ EVs have recently been characterized in
120 cerebrospinal fluid (CSF) and cell culture, with changes in fluids of AD and MCI patients (62). In
121 the pigment cell amyloid model system (63), APOE was associated with EVs in the
122 multivesicular body, where it nucleated formation of cytotoxic amyloid aggregates (59,64)
123 before release from the cell. APOE is prominently sorted into EVs, particularly from neurons
124 and astrocytes (58). APOE shuttling may increase upon exposure to Aβ peptides (58). Consistent
125 with an influence on endosome-origin EV biogenesis, APOE is a well-known determinant of
126 transmission of certain enveloped viruses, a role exerted in the cell of origin, not the recipient
127 cell (65). Studies in the periphery have touched on the role of EVs in the context of APOE and
128 atherosclerosis (e.g., (66–68)), but without finding direct connections.
129
130 In this study, we separated and characterized EVs from human AD and control brain tissue.
131 Most studies of EVs in AD to date focus on EV functions or EV-associated biomarkers in biofluids
132 or cell culture supernatant. However, EVs are most likely to act locally, in the tissue of origin.
133 We therefore obtained brain tissue of AD cases with different APOE genotypes as well as
134 control brain tissue. We used our modification of a rigorous method for separation of tissue EVs
135 (69,70) to obtain and characterize bdEVs in accordance with the recommendations of the
136 Minimal Information for Studies of EVs (MISEV) and related initiatives of the International
137 Society for Extracellular Vesicles (ISEV) (26,71–73). RNA and protein profiling revealed multiple

138 molecular entities associated with Alzheimer's disease and, to a lesser extent, with APOE

139 genotype in AD.

140 **METHODS**

141

142 ***Tissue collection, processing, and approvals***

143 Human brain tissues were obtained from Johns Hopkins Alzheimer's Disease Research Center.
144 All collections were approved by the Johns Hopkins University Institutional Review Board.
145 Following external examination and weighing of the autopsy brain, the right cerebral
146 hemisphere was cut in coronal slabs and frozen on prechilled metal plates and stored at –80°C.
147 A mixture of temporal cortex and inferior parietal cortex tissues from 23 Alzheimer's disease
148 (AD) patients and 7 non-AD controls were included in the study (Table 1). AD patients were
149 diagnosed according to Braak (74) and CERAD (75,76) criteria. For APOE genotyping, genomic
150 DNA was extracted from tissue using the DNeasy kit (Qiagen). Genotyping was performed using
151 standard procedures (77).

152

153 ***Separation of extracellular vesicles from brain tissue***

154 EVs were separated from brain tissues using our published protocol (70). Before extraction, a
155 small (~50 mg) piece of tissue was stored at −80°C for later protein and RNA extraction. The
156 remaining frozen tissue was weighed and briefly sliced on dry ice and then incubated in 75 U/ml
157 collagenase type 3 (Worthington #CLS-3, S8P18814) in Hibernate-E solution for 20 min at 37°C.
158 PhosSTOP and Complete Protease Inhibitor (SigmaAldrich PS/PI 4906837001/11697498001)
159 solution were added to stop digestion. The dissociated tissue was spun at 300 × g for 10 min at
160 4°C. Supernatant was transferred to a fresh tube and spun at 2000 × g for 15 min at 4°C.
161 Supernatant was filtered through a 0.22 µm filter (Millipore Sigma, SLGS033SS) to deplete

162 tissue debris and spun at 10,000 × g for 30 min at 4°C (Thermo Fisher swinging-bucket rotor
163 model AH-650, k-factor 53, acceleration and deceleration settings of 9, using Ultra-Clear tubes
164 with 5 ml capacity). The pellet was resuspended in 100 µl PBS. This resuspension is termed the
165 "10,000 × g pellet" (10K). The 10,000 × g supernatant was concentrated by 100 kilodalton (kDa)
166 MWCO protein concentrator (Thermo Fisher 88524) from 5 ml to 0.5 ml and loaded onto a size-
167 exclusion chromatography column (qEV original, IZON Science SP1-USD, Christchurch, New
168 Zealand) and eluted by PBS. 0.5 ml fractions were collected. The first 3 ml (Fractions 1-6) of the
169 eluate were discarded as the void volume and subsequent 0.5 mL fractions were collected. For
170 the purposes of this study, a total of 2 ml eluate (Fractions 7-10) were pooled and
171 ultracentrifuged for 70 min at 110,000 × g (average) at 4°C (swinging-bucket rotor model TH-
172 641, Thermo Fisher, k factor 114 at max speed, acceleration and deceleration settings of 9,
173 using thinwall polypropylene tubes with 13.2 ml capacity). Supernatant was removed, and the
174 pellet was resuspended in 100 µl PBS as the purified EV fraction. Fractions were stored at -80°C.
175

176 ***Brain homogenate preparation for protein and RNA***

177 For protein extraction, brain homogenates (BH) were prepared by grinding tissue in cold PBS
178 containing PI/PS with a handheld homogenizer (Kontes Pellet Pestle Motor) for 10 sec. RIPA
179 lysis buffer (Cell Signaling Technology 9806) was added and the mixture was sonicated using an
180 ultrasonic ice bath at 20 kHz for 4 × 20 sec, with a 10 sec interval between each sonication.
181 Homogenate was rotated at 4°C for 2 h and spun 15 min at 14,000 × g at 4°C. Supernatant was
182 transferred to tubes and stored at -80°C.

183 For RNA extraction, Trizol (Thermo Fisher 15596018) was added to frozen brain tissue and
184 homogenized with Lysing Matrix D beads (MP Biomedicals 116913100) using a benchtop
185 homogenizer at speed setting of 4.0 m/s for 20 sec (FastPrep-24, MP Biomedicals). After
186 homogenization, the supernatant was collected and subjected to RNA extraction by miRNeasy
187 Mini Kit (Qiagen 217004) according to the manufacturer's instructions.
188
189 ***Nano-flow analysis***
190 EV concentration and size distribution were estimated using the nanoFCM flow nanoAnalyzer
191 (NanoFCM Co.) per manufacturer's instructions. The instrument was calibrated for
192 concentration and size using 200 nm polystyrene beads and a silica nanosphere cocktail
193 (provided by NanoFCM as pre-mixed silica beads with diameters of 68, 91, 113, and 151 nm),
194 respectively. EV and 10K preparations were resuspended in 50 µl of PBS, diluted as needed
195 (typically 1:200 dilution for EV and 1:50 dilution for 10K fractions), and loaded and recorded for
196 1 minute. Using a calibration curve, the flow rate and side scatter intensity were converted into
197 particle numbers.
198
199 ***RNA extraction and quality control***
200 RNA was extracted by miRNeasy Mini Kit (Qiagen 217004) according to the manufacturer's
201 instructions. The small RNA profiles of samples were analyzed using capillary electrophoresis by
202 RNA 6000 Pico Kit (Agilent Technologies 5067-1513) on a Fragment Analyzer (Advanced
203 Analytical). Total RNA and small RNA from BH were analyzed using capillary electrophoresis by
204 RNA 6000 Nano Kit (Agilent Technologies 5067-1511) and RNA 6000 Pico Kit.

205

206 ***Small RNA sequencing***

207 EV RNA was concentrated to 6 µl using a Savant SpeedVac Vacuum concentrator. Small RNA
208 libraries were constructed from 50 ng of RNA extracted from brain homogenate or 5 µl of RNA
209 from bdEVs using the Ion Total RNA-Seq Kit V2 (Life Technologies 4475936). Barcodes were
210 attached using the Ion Xpress™ RNA-Seq Barcode 1-16 Kit (Life Technologies 4471250)
211 according to the manufacturer's protocol and as previously published (78). The yield and size
212 distribution of the small RNA libraries (96 nt to 250 nt) were assessed using the Agilent 2100
213 Bioanalyzer™ instrument with DNA 1000 chip (Agilent Technologies 5067-1504). Multiplexed
214 libraries were equally pooled to 45 pM and prepared for deep sequencing using the Ion Chef
215 system (Life Technologies 4484177) and sequenced on the Ion Torrent S5™ using Ion™ 540
216 chips (Life Technologies A27765).

217

218 ***RNA sequencing data analysis***

219 Original BAM files were converted into FASTQ format using picard tools (SamToFastq
220 command). Reads shorter than 15 nt were removed from the raw FASTQ data using cutadapt
221 software v1.18. The size-selected reads were aligned to human reference transcriptomes using
222 bowtie software (1 mismatch tolerance) in a sequential manner. Specifically, reads were first
223 mapped to rRNA, tRNA, RN7S, snRNA, snoRNA, scaRNA, VT-RNA, Y-RNA as well as the
224 mitochondrial genome. All reads which did not map to the above RNA species were aligned to
225 human miRNA references (miRBase 22 release). The remaining reads were further aligned to
226 protein-coding mRNAs and long non-coding RNA (lncRNA) references (GENCODE Release 29).

227 The numbers of reads mapped to each RNA type were extracted using eXpress software based
228 on a previous publication (79). To compare the RNA biotype distribution, reads of different RNA
229 biotypes were normalized as reads per million total reads (RPM). Differential gene expression
230 was quantified using R/Bioconductor packages DESeq or DESeq2 as described (80,81).
231
232 ***Mass spectrometry***
233 Samples were resuspended in 1 X RIPA buffer (20mM Tris-HCl pH7.5, 150mM NaCl, 1mM
234 Na2EDTA, 1mM EGTA, 1% NP-40, 1% SDS, 2.5mM sodium pyrophosphate, 1mM β-
235 glycerophosphate, 1mM Na3VO4, 1µg/ml leupeptin) and protease inhibitors and incubated on
236 ice for 5 min. The samples were sonicated for 15 min in an ice water bath before centrifugation
237 at 14,000 × g at 4°C for 10 min. The supernatant was collected and assessed for protein
238 concentration using the micro BCA assay (Thermo Fisher Scientific 23235). 3 µg of brain
239 homogenate and 1.5 µg of 10K pellet and EV samples were buffer-exchanged prior to mass
240 spectrometry to remove detergent. Proteins were resuspended in 8M Urea, 50 mM Tris pH=8.3.
241 1 µL of TCEP (tris [2-carboxyethyl] phosphine hydrochloride, 200 mM solution in water) was
242 then added to the samples and incubated for 4 hours at 21°C in a ThermoMixer (Eppendorf
243 AG). 4 µL of 1M IAA (iodoacetamide in water) was then added and samples were incubated in
244 the dark at 21°C. 800 µL of 50 mM Tris (pH 8.3) and 1 µg trypsin were then added to samples
245 prior to overnight incubation at 37°C. 10 µL of 10% trifluoroacetic acid (TFA) was added to each
246 sample to acidify. Samples were cleaned using stage-tips preparations using 3 plugs of Empore
247 polystyrenedivinylbenzene (SBD-XC) copolymer disks (Sigma Aldrich, MO, USA) for solid phase
248 extraction. Peptides were reconstituted in 0.1% formic acid and 2% acetonitrile and loaded

249 onto a trap column (C18 PepMap 100 µm i.d. × 2 cm trapping column, Thermo Fisher Scientific)
250 at 5 µL/min for 6 min using a Thermo Scientific UltiMate 3000 RSLCnano system and washed for
251 6 min before switching the precolumn in line with the analytical column (BEH C18, 1.7 µm, 130
252 Å and 75 µm ID × 25 cm, Waters). Separation of peptides was performed at 45°C, 250 nL/min
253 using a linear ACN gradient of buffer A (water with 0.1% formic acid, 2% ACN) and buffer B
254 (water with 0.1% formic acid, 80% ACN), starting from 2% buffer B to 13% B in 6 min and then
255 to 33% B over 70 min followed by 50% B at 80 min. The gradient was then increased from 50%
256 B to 95% B for 5 min and maintained at 95% B for 1 min. The column was then equilibrated for
257 4 min in water with 0.1% formic acid, 2% ACN. Data were collected on a Q Exactive HF (Thermo
258 Fisher Scientific) in Data Dependent Acquisition mode using m/z 350–1500 as MS scan range at
259 60 000 resolution. HCD MS/MS spectra were collected for the 7 most intense ions per MS scan
260 at 60 000 resolution with a normalized collision energy of 28% and an isolation window of 1.4
261 m/z. Dynamic exclusion parameters were set as follows: exclude isotope on, duration 30 s, and
262 peptide match preferred. Other instrument parameters for the Orbitrap were MS maximum
263 injection time 30 ms with AGC target $3 \times 10^6$, MSMS for a maximum injection time of 110 ms
264 with AGT target of $1 \times 10^5$.
265
266 ***Proteomics data analysis***
267 Human protein sequences (last modified date: 16 May 2019) were downloaded from the
268 Uniprot database and used as the database for the search engine. Common Repository of
269 Adventitious Proteins (CRAP) was used as the potential lab contaminant database. Protein
270 identification was performed using the proteomics search engine Andromeda built in to

271 Maxquant V 1.16.0. Trypsin with a maximum of two missed cleavages was used as the cleavage
272 enzyme. Carbamidomethyl of cysteine was set as fixed modification and oxidation of
273 methionine was set as variable modification. The Percolator results were set to reflect a
274 maximum of 1% false discovery rate (FDR). The Label Free quantification was done with match
275 between runs using a match window of 0.7 min. Large label free quantification (LFQ) ratios
276 were stabilized to reduce the sensitivity for outliers. For human datasets, data scaling was done
277 using the cyclic loess method, and scaled data were visualized with a PCA plot. For differential
278 abundance analysis, nested factorial design was set up for the analysis, where each subtype of
279 the disease was nested within the main disease category and contrasts for the main categories
280 were computed by averaging the subtypes.
281
282 The protein interaction and cluster protein function prediction was done by Protein-Protein
283 Interaction Networks Functional Enrichment Analysis (STRING) (82). Kyoto Encyclopedia of
284 Genes and Genomes (KEGG) (83) was used to enrich pathway involvement of identified
285 proteins. Statistical significance of enrichment was determined by the tools mentioned above.
286 Only nominally significant categories (false discovery rate (FDR) < 0.05) were included for
287 analysis.
288
289 **Electrochemiluminescence-linked (ECL) immunoassay for total tau and phosphorylated tau**
290 **detection**
291 Total tau and phosphorylated tau at threonine 231 (phosTau) were measured in BH, 10K, and
292 EVs using an ECL-immunoassay (Meso Scale Discovery K15121D) according to the

293 manufacturer's instructions. In brief, 10K and EV samples were diluted 1:10 while BH was
294 diluted 1:100 in 2% block buffer (2% BSA in tris buffer) containing 0.5% triton X-100. Samples
295 were incubated for one hour on the plate. After washing the plate, the SULFO-TAG Anti-Total
296 Tau Antibody was added and incubated with the plate for one hour. After washing, MSD Read
297 Buffer was added, and the plate was read immediately with a Quick plus SQ 120 MM
298 instrument. Data analysis was done on MSD DISCOVERY WORKBENCH software version 2.0.
299
300 ***Statistical analysis***
301 Statistical significance of particle count, particle: protein ratio, size distribution, RNA biotype
302 differences, and tau and phosTau level differences between AD and control groups and
303 between either of two APOE genotype groups were determined by two-tailed Welch's t-test.
304
305 ***Data availability***
306 Nucleic acid sequencing data have been deposited with the Gene Expression Omnibus,
307 accession GSE159541. Proteomics data files are available on request. We have submitted all
308 relevant details of our experiments to the EV-TRACK knowledgebase (EV-TRACK ID: EV200126)
309 (73).
310
311

312 **RESULTS**

313

314 ***Separation of EVs from AD and control brain tissue***

315 Following the protocol illustrated in Figure 1A, we separated brain-derived extracellular vesicles
316 (bdEVs) from control (n=7) and AD (n=23) individuals with different APOE genotypes (Table 1).
317 A small amount (~50 mg) of each tissue was set aside to produce brain homogenate (BH) to
318 assess protein and RNA profiles of the source material. After enzymatic digestion of the
319 remaining tissue and initial filtering, 10,000 x g ultracentrifuged pellets were collected and
320 termed "10K" as an intermediate product of EV separation. The 10K supernatant was then
321 separated by size exclusion chromatography (SEC) (70) and concentrated into a more pure EV
322 preparation. Fractions were processed for characterization, including proteomics and small RNA
323 profiling.

324

325 ***Basic EV characterization***

326 Particle concentration per 100 mg tissue input and particle size distribution were determined
327 by nano-flow cytometry measurement (NFCM). No significant particle yield difference was
328 detected between AD and control brain-derived 10K and EV fractions (Figure 1B left).
329 Particle:protein ratio was also calculated to evaluate EV purity. This ratio was similar between
330 AD and control group (Figure 1B right). However, the EV fraction had a higher particle:protein
331 ratio compared with 10K, as expected and consistent with greater protein contamination of the
332 10K pellet (Figure 1B right). Fractions from AD and control groups also had similar size
333 distributions. However, more small particles in the approximately 45-50 nm diameter range

334 were observed in AD samples compared with controls (Figure 1C). No significant particle count
335 differences or size distribution shifts were observed for samples with different APOE genotypes
336 (ε2/3, ε3/3, ε3/4/, and ε4/4; Figure S1A-B). We examined the expression levels of 13 proteins
337 that are commonly reported to be associated with EVs (CD81, CD9, FLOT1, FLOT2, RAB1A,
338 RAB7A, TUBA1B, TUBB4B, ANXA2, ANXA5, ANXA6, ACTN1, GAPDH). These proteins were not
339 found to be significantly differentially abundant between AD and controls. Principal component
340 analysis (PCA) also showed different EV marker expression patterns between BH, 10K, and EV
341 fractions, but not between AD and controls (Figure 1D).
342
343 ***Assessment of RNA biotype distribution***
344 Small RNA sequencing of BH, 10K, and EV fractions yielded 3.2M (± 1M), 2.2M (± 0.9M), and
345 0.75M (± 0.36M) reads, respectively (M = million, 1 x 10^6). After adapter clipping and
346 removing reads shorter than 15 nt, 71.28% (± 4.4%) of BH, 73.79% (±6.8%) of 10K, and 41.83%
347 (± 9.0%) of EV reads mapped to the human genome (hg38). Reads mapped to various RNA
348 biotypes were normalized to reads per million mapped reads (RPM) (Fig S2A-C). Overall, no
349 major differences in biotype distribution were observed between AD and control conditions,
350 although AD EVs showed a slight decrease in mitochondrial RNA (mtRNA) (Figure S2C). We then
351 determined enrichment of ncRNA biotypes in EVs relative to tissues and assessed whether the
352 enrichment pattern differed between AD and control brains. To do this, we normalized the RPM
353 of each ncRNA biotype to its average RPM in brain tissues (Figure S2D). Consistent with earlier
354 reports (70,84–86), miRNA and snoRNA were relatively underrepresented in EVs compared with
355 brain homogenates. The same was observed for mtRNA and, to a lesser extent, for snRNA. Y-

356 RNA was equally abundant in BH, 10K, and EVs. tRNA was enriched in 10K and was equally
357 abundant in EVs and BH. RN7S (SRP-RNA) was significantly enriched in the purified EV fraction
358 of AD samples, but not of controls. Vault RNAs were strongly enriched in EVs, although this may
359 have been due to co-purification of extracellular Vault particles with EVs, as reported earlier
360 (87). Interestingly, both protein-coding (mRNAs) and long non-coding RNAs (lncRNAs) were
361 enriched in EVs compared with BH and 10K, and these reads mapped to thousands of different
362 genes. However, because of our size selection and library preparation methods, these reads
363 likely represent the RNA degradome and not full-length RNAs.
364
365 ***EVs are associated with differentially expressed miRNAs related to AD pathology***
366 Examining individual miRNAs, 26 miRNAs (10K) and 16 miRNAs (EVs) differed significantly (FDR
367 < 0.05) between AD and controls (Figure 2A). Of these, two miRNAs in 10K and nine miRNAs in
368 EVs differed by more than two-fold (Figure S3A-B). Table 2 provides a summary of these
369 dysregulated miRNAs, indicating up/downregulation and involvement in AD as reported in
370 previous studies, since up/downregulation of some EV-associated miRNAs was consistent with
371 reports of brain tissue expression (54–56). By APOE genotype, focusing on the presumed
372 highest-risk ε4/4 and the lowest-risk ε2/3 carriers in our study, nine miRNAs in 10K differed
373 more than two-fold (with p value < 0.05), while only two miRNAs (miR-379-5p and miR-199a-
374 5p) differed in EVs (Figure 2B, S4A-B, and Table 3). However, none of the same miRNAs were
375 found in the comparisons of AD versus controls and APOE ε4/4 versus ε2/3.
376

377 To assess whether AD-associated miRNA differences in the extracellular space reflect overall
378 changes in brain tissue, we compared miRNA fold-changes of 10K and EVs with BH. We
379 highlighted miRNAs that were differentially abundant only in BH (blue dots, Figure 2C), only in
380 10K or EV (red dots), or in both EVs and BH (purple dots). Around 30% of differentially abundant
381 EV miRNAs reflected differences that could also be observed in BH (18 miRNAs in 10K and 13 in
382 EV, Figure 2C). miRNAs that showed robust differential abundance (FDR < 0.05 and log2 fold-
383 change > 2) were found within this subset of miRNAs. Eight miRNAs showed consistent changes
384 across BH, 10K, and EVs (Figure 2D). Analyzing the higher- and lower-risk APOE genotypes as
385 above, more than 90 miRNAs were differentially abundant in BH (blue dots), while relatively
386 few miRNAs differed in EVs (red dots). Of the differentially abundant miRNAs, 14 showed
387 consistent change between 10K and BH, but only three between EVs and BH (Figure 2E).
388 Curiously, the red blood cell-specific miR-451a was consistently differentially abundant across
389 all fractions (Figure 2F). Whether this is a coincidental contaminant or indicative of some
390 biological difference may require further investigation. miR-328-2p, in contrast, was
391 downmodulated in BH and 10K, but upmodulated in the EV fraction (Figure 2F).
392
393
394 ***Differential expression of other non-coding RNA biotypes in brain tissue and EVs related to AD***
395 ***pathology***
396 Since incorporation into EVs of non-miRNA non-coding RNAs can be modulated by external
397 stimuli imposed on cells (86,88), and since these ncRNAs may also contribute to intercellular
398 communication (89,90), we examined individual snoRNAs, snRNAs, Y-RNAs, and tRNAs.

399 snoRNAs were relatively depleted from EVs (Figure S2D), and we did not find any significant
400 differences in snoRNA content of BH, 10K or EVs in AD versus controls (data not shown).
401 Additionally, no differences in snRNA were found for 10K or EVs in AD versus controls, although
402 a significant upregulation of RNU4-2 in AD brain homogenates was observed (Figure S5A). We
403 also observed slight differences in Y-RNA content of AD versus control EVs (Figure S5B).
404 Compared with non-AD controls, 10K fractions of AD patients had higher levels of Y4-RNA (p
405 value < 0.05), while EVs contained lower levels of Y1-RNA (p value < 0.05).
406
407 Interestingly, we found many differences in tRNA content of EVs in AD versus controls (Figure
408 3A). Most of these differences were subtle, however, as none of the tRNAs were enriched more
409 than twofold. In EVs, we observed changes in various isodecoders of tRNA-Cys-GCA and tRNA-
410 Gly-GCC. Additionally, we observed changes in tRNA-Val, tRNA-Arg, tRNA-Pro, and different
411 tRNA-Ala isoacceptors. In contrast, no clear differences in tRNA content were found in 10K.
412 Next, we compared the tRNA content of 10K and EVs from APOE ε4/4 versus ε/3 carriers
413 (Figure 3B). The fold-differences in tRNA dependent on APOE genotype were larger than those
414 dependent on AD status, although fewer significant tRNAs were found. Two tRNA-Gly-CCC
415 isodecoders were enriched in 10K from APOE ε2/3 carriers, while no significant differences
416 were observed in EVs (as defined by FDR < 0.05).
417
418 We subsequently compared the differences in EV-associated tRNA with differences in brain
419 homogenates (Figure 3C). Like the miRNAs, most of the differences were observed only in the
420 brain homogenates, or in EVs, while a minor number of tRNAs differed in both. Comparing

421 APOE genotype-dependent differences in the tRNA content of EVs and BH, we observed a great
422 difference in BH, or in EVs, but only a small number of tRNAs that differed in both (Figure 3D).
423
424 **Proteomics and regulatory pathways**
425 Analysis of data collected by label-free mass spectrometry identified 1675, 801, and 1197
426 proteins in BH, 10K, and EVs (Supplemental Table 1), respectively. Most proteins were
427 identified in both AD and control in BH (73.6%), 10K (66.5%), and EVs (66.6%) (Figure 4A, Figure
428 S6A). Enrichment of common and AD "unique" proteins in BH, 10K, and EVs according to
429 presumed regulatory pathways as identified in the Kyoto Encyclopedia of Genes and Genomes
430 (KEGG) database was observed for pathways directly or indirectly related to neurodegenerative
431 diseases (Figure 4B, Figure S6B). Metabolic pathways (e.g., carbon metabolism, glycolysis, and
432 oxidative phosphorylation) were widely enriched for common and AD-unique proteins. Proteins
433 with known involvement in Alzheimer's disease, Parkinson's disease, and Huntington's disease
434 were enriched in AD-unique proteins in 10K and EVs (Figure 4B) and common proteins in BH
435 (Figure S6B). Principal component analysis (PCA) of the EV proteome content showed a
436 separation of AD and control groups (Figure 4C, right). In contrast, no such separation was
437 observed for 10K (Figure 4C, left) or BH (Figure S6C).
438
439 **Differentially abundant proteins: AD versus control**
440 Label-free quantitation (LFQ) was used to identify up- and downregulated proteins in AD (Figure
441 4D and Figure S6D). More proteins were up- or downregulated in AD in the EV fraction (Figure
442 4D, right) than in 10K (Figure 4D left) or BH (Figure S6D). EVs have increased potential to

443 indicate the difference between AD and controls as compared with 10K and BH. Three proteins
444 (10K) and 11 proteins (EVs) differed by more than two-fold between AD and control (Figure 4E,
445 S7A-B). Examining proteins that were differentially abundant in EVs by Protein-Protein
446 Interaction Networks Functional Enrichment Analysis (STRING), 18 out of 31 had high protein to
447 protein interaction confidence scores (0.7 on a scale of 0-1), participating in AD-related
448 processes such as neurodegeneration, neurotrophin signaling, oxidative regulation, and
449 metabolic regulation (Figure 4F). Prominent among these was microtubule-associated protein
450 tau (MAPT), which forms neurofibrillary tangles in AD brains. To validate these results, we next
451 measured the concentration of total tau and tau with phosphorylated threonine 231 (phosTau)
452 in lysed BH, 10K, and EVs by ECL-immunoassay. Normalized to total protein input, both total tau
453 and phosTau were significantly increased in bdEVs of AD versus controls, but not in the 10K
454 fraction (Figure 5A). In BH, only phosTau was significantly increased in AD compared with
455 controls (Figure 5A). Results were similar when data were normalized by starting amount of
456 tissue (Figure S8). We then assessed the possible correlations of tau or phosTau in BH and 10K
457 or EV fractions. No strong correlation was observed for total tau levels (BH vs 10K or EVs;
458 Figure 5B) or for phosTau in BH and 10K. However, phosTau levels in BH and EVs were positively
459 correlated (R=0.48, p=0.007; Figure 5B).
460
461 **Proteomics: APOE ε4/4 and APOE ε2/3**
462 The analyses above were next restricted to APOE ε4/4 and ε2/3 genotypes (AD samples only).
463 Most proteins were detected in more than 50% of individuals in each group (i.e., n > 3 in each;
464 Figure 6A, Figure S9A). Most proteins were found in common in the ε4/4 and ε2/3 groups

465 (71.4% in 10K, 70.3% in EVs, and 81.5% in BH). KEGG pathway analyses of APOE ε4/4-"unique"
466 proteins in 10K and EVs corresponded with metabolism-related pathways (carbon, glutathione,
467 and galactose metabolism) (Figure 6B). KEGG pathway analysis of APOE ε2/3-"unique" proteins
468 in 10K and EVs did not return enriched pathways (data not shown), although numerous
469 pathways were enriched in BH of APOE ε2/3 carriers (Figure S9B). Moreover, both ε4/4 and
470 ε2/3 contained enriched proteins in BH that were involved in Alzheimer's disease, Huntington's
471 disease, and oxidative phosphorylation (Figure S9B).
472
473 The fold changes and p values of individual proteins upregulated and downregulated in ε4/4 vs
474 ε2/3 are shown in Figure 6C (10K and EVs) and Figure S9C (BH). The expression levels of
475 dysregulated proteins between ε4/4 vs ε2/3 are shown in Figure 6D and Figure S10A-B. As for
476 AD pathology overall, more differentially expressed proteins were identified in 10K and EVs
477 than in BH. The potential functions of these proteins in neurodegenerative disease progression
478 are summarized in Tables 4 and 5.
479
480

481 **DISCUSSION**

482

483 The roles of EVs in regulating CNS diseases have been inferred predominantly from studies of *in*
484 *vitro* models and biofluid EVs, with growing but still limited study of tissue EVs. Here, we
485 compared protein and small RNA contents of brain homogenate with those of a "10K" pelleted
486 extracellular fraction and a purified EV fraction of control and late-stage AD brain, including
487 several APOE genotypes. Although the concentrations of recovered particles did not differ
488 significantly with AD pathology, several bdEV miRNAs, tRNAs, and proteins were dysregulated
489 not only between AD and controls, but also between the APOE genotypes representing the
490 most "distant" risk groups in our study, the ε4/4 and ε2/3 carriers. Proteome differences
491 between AD and controls were most pronounced for EVs, suggesting that EV proteins may have
492 the best biomarker potential, at least for late-stage AD. The dysregulated molecules identified
493 in our study, especially those involved in aging and neurodegeneration pathways, may be
494 involved in CNS disease mechanisms and constitute new biomarkers for disease monitoring.

495

496 **Does AD or APOE genotype affect EV production?**

497 Consistent with previous studies on bdEVs from human cortex (91,92), we observed a similar
498 bdEV recovery for AD and control. However, since bdEVs are released as a mixture of various
499 subtypes and from diverse cells, this finding does not exclude the possibility that biogenesis of
500 specific EV subtypes may be affected by AD. For example, MHC class I bdEVs were reportedly
501 enhanced in preclinical AD patients compared with controls and late-stage AD (92). Also, the
502 APOE ε4 allele was reported to be involved in neuronal, endosomal, and lysosomal system

503 dysfunction (93). In another study, control brain tissues from human and mouse had reduced
504 EV counts in the presence of the APOE ε4 allele (61). However, in our late-stage AD samples
505 (Braak stage 5-6, CERAD B-C), no particle concentration difference was associated with the
506 APOE ε4 allele or other variants. Consistent with previous findings, this suggests that effects of
507 APOE alleles, if present, may affect EVs and their effects on brain function in a measurable
508 manner only before late-stage disease (13,94). Further studies of APOE will be needed in young
509 brain and during early disease stages.
510
511 **Altered bdEV miRNA expression in AD**
512 RNA sequencing revealed several differentially expressed (DE) miRNAs in AD bdEVs with
513 potential involvement in AD. Importantly, these DE miRNAs largely overlapped with results of
514 earlier studies on miRNAs in AD brain tissues (54–56). For example, miRNA-132-3p was
515 downregulated in AD EVs. It was previously found to be downregulated in late-onset AD,
516 negatively correlated with Braak stages and formation of tau tangles in the prefrontal cortex
517 (55). miR-132 promotes neurite outgrowth and synapse formation (95,96), with expression
518 driven by the neurotrophin-responsive transcription factor CREB (97). Additionally, miR-132
519 knockout mice express increased levels of phosphorylated tau (98) and display memory deficits
520 (99). In line with downregulated miR-132-5p, we found that tau levels were increased in AD
521 EVs. Two other miRNAs downregulated in AD EVs (miR-485-3p and miR-338-5p) target beta-
522 secretase 1 (BACE1) (100,101). Together with γ-secretase, BACE1 cleaves APP into aggregate-
523 forming Aβ peptides (102). Downregulated miR-129-5p and miR-432-5p regulate
524 neuroinflammation (103,104), and miR-129-3p targets fragile X mental retardation 1 (FMR1),

525 which controls migration of cortical neurons (105,106). Although our study predominantly
526 highlights downregulated miRNAs, upregulated miRNAs have also been reported in AD bdEVs
527 (107). We found at least three upregulated miRNAs in common with that study: miR-483-5p,
528 miR-152-3p, and miR-30a-5p (107). Beyond these validations, differences between the studies
529 may be explained by use of different brain regions for bdEV isolation, as well as differences in
530 separation methods, possibly affecting purity and recovery of EV subtypes. Overall, we found
531 various dysregulated miRNAs in AD EVs that appear to be involved in AD hallmarks such as APP
532 and tau processing, neuronal function, memory formation, and neuroinflammation.
533
534 **bdEV miRNAs and APOE genotype**
535 In contrast with AD versus control comparisons, EV miRNA profile differences by APOE were not
536 as pronounced. Nevertheless, several EV-associated miRNAs differed. In the 10K fraction of
537 APOE ε4/4 carriers, miR-29b-5p was downregulated. This miRNA targets BACE, which
538 contributes to Aβ aggregation (Hebert et al PNAS 2008). Additionally, we observed
539 downregulation of miR-379-5p and miR-410-3p, which have been previously implicated in
540 anxiety behavior (108), miR-23a-5p, which is linked to neuronal cell loss (109), and miR-483-5p,
541 which is involved in neuronal development (110). Our findings are limited, however, since only
542 late-stage carriers were examined, with late Braak stage and similar CNS pathology. miRNAs are
543 quite possibly involved in APOE genotype interactions much earlier in AD, perhaps even in
544 young, putatively healthy individuals. More research is thus needed to address the involvement
545 of these miRNAs in AD pathogenesis.
546

547 **AD-dependent differences in additional bdEV-associated ncRNAs**

548 AD-dependent differences in bdEV-associated ncRNAs such as tRNAs and Y-RNAs were also
549 apparent. These ncRNAs are highly abundant in EVs from various sources (84–86,111–113), but
550 their roles in health and disease remain largely unexplored. We found various AD-dependent
551 differences in tRNA content of EVs, as well as APOE-dependent differences in tRNAs in the 10K
552 fraction. Changes in cellular tRNA abundance have been implicated in neurological disorders
553 (114,115), and dysregulation of cellular tRNA levels affects protein expression in cancer (116).
554 Interestingly, tRNA fragments released with EVs may modulate gene expression in recipient
555 cells (117). Small changes in bdEV-associated Y-RNAs (Y1 and Y4) were also observed. Y-RNA is
556 abundantly detected in EVs from various biological sources (118). Cellular Y-RNA serves as a
557 scaffold for RNA-binding proteins (119). In AD patients, dysregulation of Y3-RNA binding to
558 enhancer protein HuD (ELAVL4) was shown to cause alternative splicing in neurons (120).
559 Additionally, EV-associated Y4-RNA activated endosomal RNA sensor TLR7 in monocytes (90). In
560 brain tissue of AD patients, we observed a significant difference in U4 RNA, which has not been
561 previously reported in AD. As part of the spliceosome complex, U4 is involved in pre-mRNA
562 splicing (121). In the prefrontal cortex of AD brains, snRNA U1 was found to be upregulated and
563 to accumulate in tau plaques (122,123). Upregulation of U1 was additionally implicated in
564 aberrant mRNA splicing and altered APP expression (122). Our findings encourage further
565 investigations into the role of extracellular non-miRNA ncRNAs in AD and other neurological
566 conditions.

567

568 **Implications of bdEV-associated proteins in AD**

569 ***bdEV-associated tau proteins***

570 EVs have been widely reported to propagate misfolded protein MAPT (tau) in
571 neurodegenerative disease (42,124–126). Consistent with other bdEV studies (42,91,125), we
572 found a higher level of tau and phosTau protein in EVs of AD brain compared with controls,
573 adding more evidence to EV-mediated tau propagation. However, we did not see consistent
574 associations with APOE genotype, possibly because our samples sizes were small, and possibly
575 because we examined brains from individuals with late-stage disease. Further study is needed,
576 including study of younger and early-stage individuals with different genotypes, to decide if EVs
577 act as a protective factor to clear tau from the CNS to the periphery, or as a neurotoxic factor to
578 spread tau between neurons and glia, or perhaps some as-yet incompletely understood balance
579 between the two extremes.

580

581 ***bdEV-associated antioxidant proteins***

582 Upregulated members of the antioxidant peroxiredoxin (PRDX) family in AD EVs include PRDX1,
583 PRDX2, and PRDX6. Oxidative damage is often implicated in the progression of
584 neurodegenerative diseases. We and our collaborators previously found that PRDXs were highly
585 abundant in EVs derived from both human induced pluripotent stem cells (iPSCs) and
586 mesenchymal stem cells (MSCs), and that these proteins help to reduce oxidative stress in
587 induced senescent cells (127). Although the protective role of PRDX family members in AD
588 (128–130) and the association of PRDX with EVs (127,131,132) have been reported before, this
589 is the first study to show PRDXs upregulating in tissue EVs from AD brain. We also found
590 another antioxidant defense protein, deglucase DJ1 (PARK7), enriched in APOE ε4/4 compared

591 with ε2/3 samples. PARK protects cells against hydrogen peroxide-induced death (133,134)
592 upon oxidative stress. We hypothesize that this factor may spread via EVs as a neuroprotective
593 response in patients with the risk factor ε4.
594
595 ***bdEV-associated mitochondrial and metabolism pathway proteins***
596 Mounting evidence suggests that mitochondrial and metabolism dysfunction contribute to AD
597 by compromising the energy supply (135–138). We found numerous bdEV-associated proteins
598 that contribute to mitochondrial and metabolic pathways. The ATPase enzyme member valosin-
599 containing protein/p97 (VCP) was upregulated in AD bdEVs. VCP is thought to bring about
600 mitophagy impairment, leading to mitochondrial dysfunction in AD (139,140). Higher levels of
601 tricarboxylic acid cycle (TCA) protein mitochondrial aconitate hydratase (ACO2) were previously
602 found in multiple brain regions of AD patients (141) and here appeared to be enriched in bdEVs
603 of APOE ε4/4 patients compared with ε2/3. We also identified changes in bdEV proteins that
604 are involved in glycolytic and carbon metabolism, including transketolase (TKT) (142,143),
605 alpha-enolase (ENO1) (144,145), and fructose-bisphosphate aldolase A (ALDOA) (146). Further
606 exploration of protein modification and enzymatic activity of these proteins is now indicated to
607 unveil mechanisms of energy metabolism deficits in AD.
608
609 ***bdEV-associated proteins in neurogenesis***
610 Impairment of pathways involved in neurogenesis/differentiation are thought to be early
611 clinical events in aging and AD development (136,147–150). Among neurogenesis-related
612 proteins, the 14-3-3 protein family of ubiquitous phosphoserine/threonine–binding proteins is

613 highly abundant in brain and implicated in nervous system development and maintenance
614 (151–153). Our study shows dysregulation of 14-3-3 isoforms ε (YWHAE), ζ (YWHAZ), and γ
615 (YWHAG) in the 10K and EV fractions. 14-3-3 proteins indirectly regulate activation of Rho
616 family GTPases (154). Interestingly, several proteins in the Rho-GTPase cycle were also
617 dysregulated in our bdEVs, including Ras-related C3 botulinum toxin substrate 1/3 (RAC1/3),
618 and Rho GDP-dissociation inhibitors 1 and 2 (ARHGDIA, GDI2). We also found that contactin-1
619 (CNTN1) and neurofascin (NFASC), two proteins involved in axonal guidance and neuron
620 projection development (155–158), were downregulated in AD bdEVs, which may reflect
621 neurodegeneration. In addition, some neuroprotective proteins were also found to be
622 downregulated in bdEVs from APOE ε4/4 patients compared to ε2/3, such as γ-enolase (ENO2)
623 (159–161) and brevican core protein (BCAN) (162–164).
624
625 In summary, this is the first study thoroughly examining bdEV small RNA and protein content
626 from clinical AD patients with different APOE genotypes. Our results identified the composition
627 of RNAs (including miRNAs, tRNAs, and Y-RNAs) and proteins in bdEVs that varied with AD
628 pathology and APOE genotypes. These bdEV-transported molecules may play critical roles in
629 modulating AD progression and thus have potential for exploitation as biomarkers and
630 therapeutic targets.
631
632
633
634

**ACKNOWLEDGMENTS**

This work was supported in part by grants from the US National Institutes of Health: AI144997 (to KWW, with support for TAPD), MH118164 and AG057430 (to VM and KWW), by UG3CA241694 (to KWW), supported by the NIH Common Fund, through the Office of Strategic Coordination/Office of the NIH Director, and by the National Health and Medical Research Council of Australia (GNT1132604 to AFH). The Johns Hopkins Alzheimer's Disease Research Center provided tissues and is funded by P30 AG066507 (PI: M. Albert). VM and KWW gratefully acknowledge support from the Richman Family Precision Medicine Center of Excellence in Alzheimer's Disease including helpful comments and advice from founder and director Constantine Lyketsos. Thanks to: Kenneth Pienta, Johns Hopkins University School of Medicine, for access to the nanoFCM flow nanoAnalyzer platform; Mitchell Science Writing for manuscript editing and citation formatting; and the La Trobe University Comprehensive Proteomics Platform. We also thank members of the Witwer and Retrovirus Laboratories, Johns Hopkins University School of Medicine, and various members of the International Society for Extracellular Vesicles for valuable discussions and support.

**CONFLICTS OF INTEREST**

The authors report no conflicts of interest.

657 **FIGURE LEGENDS**

658

659 Figure 1. Alzheimer's disease (AD) and control brain tissue-derived EV (bdEV) enrichment and
660 characterization. (A) Workflow for bdEV enrichment, small RNA sequencing and proteomics.
661 Following digestion, centrifugation, and filtration steps, 10,000 x g pellets from AD and control
662 brain tissue (BH) (as indicated in Table 1) were collected and defined as the 10K fraction. Size-
663 exclusion chromatography (SEC) was applied to 10,000 x g supernatants to enrich EVs. RNA and
664 proteins from BH, 10K, and EVs were then isolated and subjected to small RNA sequencing and
665 mass spectrometry. (B) Left: Particle concentrations of 10K and EV fractions of AD and control
666 samples were measured by NFCM. Particle concentration for each group was normalized by
667 tissue mass (per 100 mg). Right: Ratio of particles to protein (particles/µg). Protein
668 concentrations of 10K and EV fractions were measured by BCA protein assay. Data are mean +/-
669 SD. ns: no significant difference ($p > 0.05$) between AD and control by two-tailed Welch's t-test.
670 (C) Size distributions of 10K and EV fractions (AD and control) were measured by NFCM and
671 calculated as particles in a specific size bin versus total detected particles in each sample
672 (percentage). Data are presented as mean +/- SD. *$p \leq 0.05$, ****$p \leq 0.0001$ by two-tailed
673 Welch's t-test. (D) Principal component analysis (PCA) based on extracellular vesicle (EV)
674 marker expression per proteomics analysis. EV markers used for PCA: CD81, CD9, FLOT1, FLOT2,
675 RAB1A, RAB7A, TUBA1B, TUBB4B, ANXA2, ANXA5, ANXA6, ACTN1, GAPDH. Data are presented
676 as mean +/- SD.

677

678 Figure 2. bdEV miRNAs with differential expression in AD. (A) Volcano plots showing 10K (left)
679 and EV (right) miRNA log2 fold changes (Log2FC) and p values (pval) for AD versus control. (B)
680 Volcano plots showing 10K (left) and EV (right) miRNA log2 fold changes (Log2FC) and p values
681 (pval) for APOE ε4/4 and APOE ε2/3 carriers. (A) and (B): Thresholds for two-fold change and p
682 value < 0.05 are indicated by dashed lines. Significant changes are indicated with different
683 colors. Grey: non-significant (Not Sig), black: non-adjusted p value < 0.05, and red: FDR < 0.05.
684 (C) miRNA log2 fold changes (Log2FC) for AD and control for BH were plotted against 10K
685 (upper left) and EVs (upper right). Venn diagrams of miRNAs differentially expressed between
686 AD and controls in 10K (bottom left) versus BH, and EVs versus BH (bottom right). (D) The
687 normalized abundance of eight miRNAs dysregulated in AD and control in common in BH, 10K,
688 and EV fractions. Data are presented as mean +/- SD. (E) miRNA log2 fold changes (Log2FC)
689 between APOE ε4/4 and APOE ε2/3 in BH were plotted against 10K (upper left) and EVs (upper
690 right). Venn diagrams of miRNAs differentially expressed between APOE ε4/4 and APOE ε2/3 in
691 10K (bottom left) versus BH, and EVs versus BH (bottom right). (C) and (E): Dashed lines indicate
692 log2FC of one (up or down). Colored dots indicate miRNAs with p values < 0.05 in BH (blue), in
693 10K/EV (red), or in both BH and 10K/EVs (purple), or unchanged transcripts (grey). Dot size
694 represents the mean normalized abundance of individual miRNAs. (F) The normalized
695 abundance of two miRNAs dysregulated in APOE ε4/4 vs APOE ε2/3 in BH, 10K, and EV
696 fractions. Data are presented as mean +/- SD.
697
698 Figure 3. bdEV tRNAs with differential expression in AD. (A) Volcano plots showing 10K (left)
699 and EV (right) tRNA log2 fold changes (Log2FC) and p values (pval) for AD versus control. (B)

700 Volcano plots showing 10K (left) and EV (right) tRNA log2 fold changes (Log2FC) and p values
701 (pval) for APOE ε4/4 versus APOE ε2/3. (A) and (B): Thresholds for two-fold change and p value
702 < 0.05 are indicated by dashed lines. Significant changes are indicated with different colors.
703 Grey: non-significant (Not Sig), black: non-adjusted p value < 0.05, and red: FDR < 0.05. (C) tRNA
704 log2 fold changes (Log2FC) for AD and control for BH were plotted against 10K (left) and EVs
705 (right). (D) tRNA log2 fold changes (Log2FC) between APOE ε4/4 and APOE ε2/3 carriers for BH
706 were plotted against 10K (left) and EVs (right). (C) and (D): Dashed lines indicate log2FC of one
707 (up or down). Colored dots indicate tRNAs with p values < 0.05 in BH (blue), in 10K/EV (red), or
708 in both BH and 10K/EVs (purple), or unchanged transcripts (grey). Dot size represents the mean
709 normalized abundance of individual tRNAs.
710
711 Figure 4. bdEV protein content reflects differences between AD and control brain tissues. (A)
712 Venn diagrams of proteins identified in 10K and EVs from AD and control patients. (B) Top 10
713 pathways ranked by FDR-corrected p value of 10K and EV proteins according to the Kyoto
714 Encyclopedia of Genes and Genomes (KEGG). (C) Principal component analysis (PCA) based on
715 proteome content of 10K (left) and EVs (right). (D) Volcano plots showing 10K (left) and EV
716 (right) protein log2 fold changes (Log2FC) and p values (pval) for AD versus control. Thresholds
717 for two-fold change and p value < 0.05 are indicated by dashed lines. Significant changes are
718 indicated with different colors. Grey: non-significant (Not Sig), black: non-adjusted p value <
719 0.05, and red: FDR < 0.05. (E) Expression level of proteins differentially expressed between AD
720 and control with fold change > 2 (non-adjusted p value < 0.05) in 10K (left) and EVs (right). Data
721 are presented as mean +/- SD. (F) String protein interaction network analysis indicated that 18

722 proteins (out of 31 proteins showing differential expression (non-adjusted p value < 0.05)
723 between AD and control in EVs) were enriched with known high confidence (0.7 on a scale of 0-
724 1) protein-protein interactions. Protein clusters are indicated with different colors based on
725 predicted functions.
726
727 Figure 5. Higher total tau and phosphorylated tau protein levels in bdEVs from AD patients
728 compared with controls. (A) The level of total tau and phosphorylated tau protein per 100 µg
729 protein input in BH, 10K, and EVs. Data are presented as mean +/- SD. ns: no significant
730 difference ($p > 0.05$), *$p \leq 0.05$, ***$p \leq 0.001$, ****$p \leq 0.0001$ by two-tailed Welch's t-test. (B)
731 Scattered plot of tau and phosphorylated tau protein levels between BH with 10K (left), and BH
732 with EVs (right) in AD and controls. Trendlines are shown in black, and the grey area depicts
733 95% confidence intervals. Pearson correlation coefficient (R) and significance (p) are shown
734 based on n = 30 AD and control samples.
735
736 Figure 6. bdEV proteins with differential expression in APOE ε4/4 and APOE ε2/3 carriers. (A)
737 Venn diagrams of proteins identified in 10K and EVs from APOE ε4/4 and APOE ε2/3 carriers.
738 (B) Significant pathways of APOE ε4/4 10K and EV proteins according to the Kyoto Encyclopedia
739 of Genes and Genomes (KEGG). (C) Volcano plots showing 10K (left) and EV (right) protein log2
740 fold changes (Log2FC) and non-adjusted p values (pval) between APOE ε4/4 and APOE ε2/3
741 carriers. Thresholds for two-fold change and p value < 0.05 are indicated by dashed lines.
742 Significant changes are indicated with different colors. Grey: non-significant (Not Sig), black:

743 non-adjusted p value < 0.05. (D) Expression level of proteins differentially expressed between
744 APOE ε4/4 and APOE ε2/3 in 10K (left) and EVs (right). Data are presented as mean +/- SD.
745
746 Figure S1. Particle yield and size distribution of bdEVs from AD samples with different APOE
747 genotypes. Particle concentration (A) and size distribution (B) of 10K and EV fractions from AD
748 patients classified by APOE genotype as measured by NFCM. Data are presented as mean +/-
749 SD. ns: no significant difference (p > 0.05) between the two APOE genotype groups by two-
750 tailed Welch's t-test.
751
752 Figure S2. Small RNA biotypes in BH, 10K, and EV fractions from AD and control patients. (A)
753 The log2 reads per million mapped reads (Log2RPM) of small RNA biotypes in BH (top), 10K
754 (middle), and EVs (bottom) of AD and control. Data are presented as mean +/- SD. **p ≤ 0.01 by
755 two-tailed Welch's t-test. (B) Normalized RNA class read counts in 10K and EVs were scaled to
756 the normalized RNA class read counts in BH. Data are presented as mean +/-SD. *p ≤ 0.05, **p
757 ≤ 0.01, ***p ≤ 0.001, ****p ≤ 0.0001 by two-tailed Welch's t-test.
758
759 Figure S3. Normalized count of miRNAs differentially expressed between AD and control with
760 fold change > 2 in 10K (A) and EVs (B) of patients classified by APOE genotype. *p value < 0.05
761 by DeSeq2 differential gene expression analysis based on the negative binomial distribution.
762

763 Figure S4. Normalized count of miRNAs differentially expressed in APOE ε4/4 versus APOE ε2/3
764 carriers with fold change > 2 in 10K (A) and EVs (B). *p value < 0.05 by DeSeq2 differential gene
765 expression analysis based on the negative binomial distribution.
766
767 Figure S5. Differential expression of RNU and Y-RNAs related to AD pathology. (A) RNU4
768 expression in AD versus control in BH. Data are presented as mean +/- SD. (B) Y-RNAs
769 differentially expressed in AD versus control in BH, 10K, and EVs. Data are presented as mean
770 +/- SD. *p ≤ 0.05 as determined by DeSeq2 differential gene expression analysis based on the
771 negative binomial distribution.
772
773 Figure S6. Proteins related to AD pathology in brain tissues. (A) Venn diagram of proteins
774 identified in BH of AD and control. (B) The top 10 pathways ranked by FDR-corrected p value of
775 BH proteins according to the Kyoto Encyclopedia of Genes and Genomes (KEGG). (C) Principal
776 component analysis (PCA) based on proteome content of BH. (D) Volcano plots showing BH
777 protein log2 fold changes (Log2FC) and p values (pval) for AD versus control. Thresholds for
778 two-fold change and p value < 0.05 are indicated by dashed lines. Significant changes are
779 indicated with different colors. Grey: non-significant (Not Sig), black: non-adjusted p value <
780 0.05, and red: FDR < 0.05.
781
782 Figure S7. Expression level of proteins differentially expressed between AD (n=23) and control
783 (n=7) with fold change > 2 in 10K (A) and EVs (B). Data are presented as mean +/- SD. *p value <
784 0.05 by Nested Factorial design differential abundance analysis.

785

786 Figure S8. Higher total tau and phosphorylated tau protein levels in bdEVs from AD patients vs

787 controls. The level of total tau and phosphorylated tau protein per 100 mg tissue input in 10K

788 and EVs. Data are presented as mean +/- SD. ns: no significant difference ($p > 0.05$), **$p \leq 0.01$

789 by two-tailed Welch's t-test.

790

791 Figure S9. Protein related to APOE genotypes in brain tissues. (A) Venn diagram of proteins

792 identified in BH from APOE ε4/4 and APOE ε2/3 carriers. (B) Volcano plots showing BH protein

793 log2 fold changes (Log2FC) and p-value (pval) for APOE ε4/4 and APOE ε2/3 carriers. Thresholds

794 for two-fold change and p value < 0.05 are indicated by dashed lines. Significant changes are

795 indicated with different colors. Grey: non-significant (Not Sig), black: non-adjusted p value <

796 0.05, and red: FDR < 0.05. (C) The pathways significant for APOE ε4/4 and APOE ε2/3 unique

797 proteins in BH according to the Kyoto Encyclopedia of Genes and Genomes (KEGG).

798

799 Figure S10. Expression level of proteins differentially expressed in APOE ε4/4 versus APOE ε2/3

800 for 10K (A) and EVs (B). Data are presented as mean +/- SD.

801 **REFERENCES**

802


803 1. About a peculiar disease of the cerebral cortex. By Alois Alzheimer, 1907 (Translated by
804 L. Jarvik and H. Greenson). Alzheimer Dis Assoc Disord [Internet]. 1987 [cited 2017 Jan
805 21];1(1):3–8. Available from: http://www.ncbi.nlm.nih.gov/pubmed/3331112

806 2. Alzheimer's Association. 2016 Alzheimer's disease facts and figures. Alzheimers Dement
807 [Internet]. 2016 Apr [cited 2017 Jan 23];12(4):459–509. Available from:
808 http://www.ncbi.nlm.nih.gov/pubmed/27570871

809 3. Reitz C. Toward precision medicine in Alzheimer's disease. Ann Transl Med [Internet].
810 2016 Mar [cited 2017 Jan 23];4(6):107–107. Available from:
811 http://www.ncbi.nlm.nih.gov/pubmed/27127760

812 4. Yankner BA, Dawes LR, Fisher S, Villa-Komaroff L, Oster-Granite ML, Neve RL.
813 Neurotoxicity of a fragment of the amyloid precursor associated with Alzheimer's
814 disease. Science [Internet]. 1989 Jul 28 [cited 2017 Jan 21];245(4916):417–20. Available
815 from: http://www.ncbi.nlm.nih.gov/pubmed/2474201

816 5. Yankner BA. Mechanisms of neuronal degeneration in Alzheimer's disease. Neuron
817 [Internet]. 1996 May [cited 2017 Jan 21];16(5):921–32. Available from:
818 http://www.ncbi.nlm.nih.gov/pubmed/8630250

819 6. Sisodia SS, St George-Hyslop PH. gamma-Secretase, Notch, Abeta and Alzheimer's
820 disease: where do the presenilins fit in? Nat Rev Neurosci [Internet]. 2002 Apr 1 [cited
821 2017 Jan 21];3(4):281–90. Available from:
822 http://www.nature.com/doifinder/10.1038/nrn785

823 7. Mattson MP. Pathways towards and away from Alzheimer's disease. Nature [Internet].
824 2004 Aug 5 [cited 2017 Jan 21];430(7000):631–9. Available from:
825 http://www.nature.com/doifinder/10.1038/nature02621
826 8. Murayama S, Saito Y. Neuropathological diagnostic criteria for Alzheimer's disease. In:
827 Neuropathology. 2004.
828 9. Stohr J, Watts JC, Mensinger ZL, Oehler A, Grillo SK, DeArmond SJ, et al. Purified and
829 synthetic Alzheimer's amyloid beta (A ) prions. Proc Natl Acad Sci [Internet]. 2012 Jul 3
830 [cited 2017 Jan 21];109(27):11025–30. Available from:
831 http://www.ncbi.nlm.nih.gov/pubmed/22711819
832 10. Watts JC, Condello C, Stohr J, Oehler A, Lee J, DeArmond SJ, et al. Serial propagation of
833 distinct strains of A  prions from Alzheimer's disease patients. Proc Natl Acad Sci
834 [Internet]. 2014 Jul 15 [cited 2017 Jan 21];111(28):10323–8. Available from:
835 http://www.ncbi.nlm.nih.gov/pubmed/24982139
836 11. Aguzzi A, Rajendran L. The Transcellular Spread of Cytosolic Amyloids, Prions, and
837 Prionoids. Neuron [Internet]. 2009 Dec 24 [cited 2017 Jan 21];64(6):783–90. Available
838 from: http://www.ncbi.nlm.nih.gov/pubmed/20064386
839 12. Vinters H V. Emerging Concepts in Alzheimer's Disease. Annu Rev Pathol Mech Dis
840 [Internet]. 2015 Jan 24 [cited 2017 Jan 21];10(1):291–319. Available from:
841 http://www.ncbi.nlm.nih.gov/pubmed/25387055
842 13. Liu C-C, Xu H, Bu G, Liu C-C, Kanekiyo T, Xu H, et al. Apolipoprotein E and Alzheimer
843 disease: risk, mechanisms and therapy. Nat Rev Neurol [Internet]. 2013 [cited 2017 Jan
844 8];9:106–18. Available from: www.nature.com/nrneurol

845 14. Thomas R, Zuchowska P, Morris AWJ, Marottoli FM, Sunny S, Deaton R, et al. Epidermal
846 growth factor prevents APOE4 and amyloid-beta-induced cognitive and cerebrovascular
847 deficits in female mice. Acta Neuropathol Commun [Internet]. 2016 Dec 27 [cited 2017
848 Jan 8];4(1):111. Available from: http://www.ncbi.nlm.nih.gov/pubmed/27788676
849 15. Saunders AM, Schmader K, Breitner JC, Benson MD, Brown WT, Goldfarb L, et al.
850 Apolipoprotein E epsilon 4 allele distributions in late-onset Alzheimer's disease and in
851 other amyloid-forming diseases. Lancet (London, England) [Internet]. 1993 Sep 18 [cited
852 2017 Jan 21];342(8873):710–1. Available from:
853 http://www.ncbi.nlm.nih.gov/pubmed/8103823
854 16. Strittmatter WJ, Saunders AM, Schmechel D, Pericak-Vance M, Enghild J, Salvesen GS, et
855 al. Apolipoprotein E: high-avidity binding to beta-amyloid and increased frequency of
856 type 4 allele in late-onset familial Alzheimer disease. Proc Natl Acad Sci U S A [Internet].
857 1993 Mar 1 [cited 2017 Jan 21];90(5):1977–81. Available from:
858 http://www.ncbi.nlm.nih.gov/pubmed/8446617
859 17. Farrer LA, Cupples LA, Haines JL, Hyman B, Kukull WA, Mayeux R, et al. Effects of age, sex,
860 and ethnicity on the association between apolipoprotein E genotype and Alzheimer
861 disease. A meta-analysis. APOE and Alzheimer Disease Meta Analysis Consortium. JAMA
862 [Internet]. [cited 2017 Jan 8];278(16):1349–56. Available from:
863 http://www.ncbi.nlm.nih.gov/pubmed/9343467
864 18. Rubinsztein DC, Easton DF. Apolipoprotein E genetic variation and Alzheimer's disease. a
865 meta-analysis. Dement Geriatr Cogn Disord [Internet]. [cited 2017 Jan 29];10(3):199–
866 209. Available from: http://www.ncbi.nlm.nih.gov/pubmed/10325447

867 19. Cutler RG, Haughey NJ, Tammara A, McArthur JC, Nath A, Reid R, et al. Dysregulation of
868 sphingolipid and sterol metabolism by ApoE4 in HIV dementia. Neurology [Internet].
869 2004 Aug 24 [cited 2017 Jan 8];63(4):626–30. Available from:
870 http://www.ncbi.nlm.nih.gov/pubmed/15326233
871 20. Hebert LE, Weuve J, Scherr PA, Evans DA. Alzheimer disease in the United States (2010-
872 2050) estimated using the 2010 census. Neurology [Internet]. 2013 May 7 [cited 2017 Jan
873 8];80(19):1778–83. Available from: http://www.ncbi.nlm.nih.gov/pubmed/23390181
874 21. Payami H, Montee KR, Kaye JA, Bird TD, Yu CE, Wijsman EM, et al. Alzheimer's disease,
875 apolipoprotein E4, and gender. JAMA [Internet]. 1994 May 4 [cited 2017 Jan
876 8];271(17):1316–7. Available from: http://www.ncbi.nlm.nih.gov/pubmed/8158809
877 22. Ungar L, Altmann A, Greicius MD. Apolipoprotein E, gender, and Alzheimer's disease: an
878 overlooked, but potent and promising interaction. Brain Imaging Behav [Internet]. 2014
879 Jun 30 [cited 2017 Jan 8];8(2):262–73. Available from:
880 http://link.springer.com/10.1007/s11682-013-9272-x
881 23. Cacciottolo M, Christensen A, Moser A, Liu J, Pike CJ, Smith C, et al. The APOE4 allele
882 shows opposite sex bias in microbleeds and Alzheimer's disease of humans and mice.
883 Neurobiol Aging [Internet]. 2016 Jan [cited 2017 Jan 21];37:47–57. Available from:
884 http://www.ncbi.nlm.nih.gov/pubmed/26686669
885 24. Raber J, Wong D, Buttini M, Orth M, Bellosta S, Pitas RE, et al. Isoform-specific effects of
886 human apolipoprotein E on brain function revealed in ApoE knockout mice: increased
887 susceptibility of females. Proc Natl Acad Sci U S A [Internet]. 1998 Sep 1 [cited 2017 Jan
888 21];95(18):10914–9. Available from: http://www.ncbi.nlm.nih.gov/pubmed/9724804

889 25. Vella LJ, Sharples RA, Nisbet RM, Cappai R, Hill AF. The role of exosomes in the processing
890 of proteins associated with neurodegenerative diseases. Eur Biophys J [Internet]. 2008
891 Mar 7 [cited 2017 Jan 21];37(3):323–32. Available from:
892 http://www.ncbi.nlm.nih.gov/pubmed/18064447
893 26. Vella L, Hill A, Cheng L. Focus on Extracellular Vesicles: Exosomes and Their Role in
894 Protein Trafficking and Biomarker Potential in Alzheimer's and Parkinson's Disease. Int J
895 Mol Sci [Internet]. 2016 Feb 6 [cited 2017 Jan 21];17(2):173. Available from:
896 http://www.ncbi.nlm.nih.gov/pubmed/26861304
897 27. Dinkins MB, Wang G, Bieberich E. Sphingolipid-Enriched Extracellular Vesicles and
898 Alzheimer's Disease: A Decade of Research. J Alzheimer's Dis [Internet]. 2016 Sep 21
899 [cited 2017 Jan 21];1–12. Available from:
900 http://www.ncbi.nlm.nih.gov/pubmed/27662306
901 28. Witwer KW, Théry C. Extracellular vesicles or exosomes? On primacy, precision, and
902 popularity influencing a choice of nomenclature. J Extracell Vesicles [Internet]. 2019 Dec
903 [cited 2019 Aug 2];8(1):1648167. Available from:
904 https://www.tandfonline.com/doi/full/10.1080/20013078.2019.1648167
905 29. Théry C, Witwer KW, Aikawa E, Alcaraz MJ, Anderson JD, Andriantsitohaina R, et al.
906 Minimal information for studies of extracellular vesicles 2018 (MISEV2018): a position
907 statement of the International Society for Extracellular Vesicles and update of the
908 MISEV2014 guidelines. J Extracell Vesicles. 2018;7(1).
909 30. Kowal J, Arras G, Colombo M, Jouve M, Morath JP, Primdal-Bengtson B, et al. Proteomic
910 comparison defines novel markers to characterize heterogeneous populations of

911 extracellular vesicle subtypes. Proc Natl Acad Sci [Internet]. 2016 Feb 23 [cited 2016 Nov
912 17];113(8):E968–77. Available from:
913 http://www.pnas.org/lookup/doi/10.1073/pnas.1521230113
914 31. Rajendran L, Bali J, Barr MM, Court FA, Kramer-Albers E-M, Picou F, et al. Emerging Roles
915 of Extracellular Vesicles in the Nervous System. J Neurosci [Internet]. 2014 Nov 12 [cited
916 2017 Jan 23];34(46):15482–9. Available from:
917 http://www.ncbi.nlm.nih.gov/pubmed/25392515
918 32. Eitan E, Hutchison ER, Marosi K, Comotto J, Mustapic M, Nigam SM, et al. Extracellular
919 vesicle-associated Aβ mediates trans-neuronal bioenergetic and Ca2+-handling deficits in
920 Alzheimer's disease models. npj Aging Mech Dis [Internet]. 2016 [cited 2017 Jan
921 23];2(1):16019. Available from: http://www.nature.com/articles/npjamd201619
922 33. Perez-Gonzalez R, Gauthier SA, Kumar A, Levy E. The exosome secretory pathway
923 transports amyloid precursor protein carboxyl-terminal fragments from the cell into the
924 brain extracellular space. J Biol Chem [Internet]. 2012 Dec 14 [cited 2016 Jan
925 22];287(51):43108–15. Available from:
926 http://www.jbc.org/lookup/doi/10.1074/jbc.M112.404467
927 34. Saman S, Kim W, Raya M, Visnick Y, Miro S, Jackson B, et al. Exosome-associated tau is
928 secreted in tauopathy models and is selectively phosphorylated in cerebrospinal fluid in
929 early Alzheimer disease. J Biol Chem [Internet]. 2011/11/08. 2012 Feb 3 [cited 2017 Jan
930 23];287(6):3842–9. Available from: http://www.ncbi.nlm.nih.gov/pubmed/22057275
931 35. Emmanouilidou E, Melachroinou K, Roumeliotis T, Garbis SD, Ntzouni M, Margaritis LH,
932 et al. Cell-Produced -Synuclein Is Secreted in a Calcium-Dependent Manner by Exosomes

933 and Impacts Neuronal Survival. J Neurosci [Internet]. 2010 May 19 [cited 2017 Jan
934 23];30(20):6838–51. Available from: http://www.ncbi.nlm.nih.gov/pubmed/20484626
935 36. Rajendran L, Honsho M, Zahn TR, Keller P, Geiger KD, Verkade P, et al. Alzheimer's
936 disease beta-amyloid peptides are released in association with exosomes. Proc Natl Acad
937 Sci U S A [Internet]. 2006 Jul 25 [cited 2017 Jan 23];103(30):11172–7. Available from:
938 http://www.pnas.org/cgi/doi/10.1073/pnas.0603838103
939 37. Fiandaca MS, Kapogiannis D, Mapstone M, Boxer A, Eitan E, Schwartz JB, et al.
940 Identification of preclinical Alzheimer's disease by a profile of pathogenic proteins in
941 neurally derived blood exosomes: A case-control study. Alzheimer's Dement [Internet].
942 2015 Jun [cited 2017 Jan 23];11(6):600-607.e1. Available from:
943 http://linkinghub.elsevier.com/retrieve/pii/S1552526014024698
944 38. Sardar Sinha M, Ansell-Schultz A, Civitelli L, Hildesjö C, Larsson M, Lannfelt L, et al.
945 Alzheimer's disease pathology propagation by exosomes containing toxic amyloid-beta
946 oligomers. Acta Neuropathol [Internet]. 2018 Jul 1 [cited 2020 Oct 16];136(1):41–56.
947 Available from: https://pubmed.ncbi.nlm.nih.gov/29934873/
948 39. Sun R, Wang H, Shi Y, Sun Z, Jiang H, Zhang J. Changes in the Morphology, Number, and
949 Pathological Protein Levels of Plasma Exosomes May Help Diagnose Alzheimer's Disease.
950 J Alzheimers Dis [Internet]. 2020 [cited 2020 Oct 16];73(3):909–17. Available from:
951 https://pubmed.ncbi.nlm.nih.gov/31884461/
952 40. Guix FX, Corbett GT, Cha DJ, Mustapic M, Liu W, Mengel D, et al. Detection of
953 Aggregation-Competent Tau in Neuron-Derived Extracellular Vesicles. Int J Mol Sci
954 [Internet]. 2018 Feb 27 [cited 2018 Mar 18];19(3):663. Available from:

955 http://www.mdpi.com/1422-0067/19/3/663

956 41. Baker S, Polanco JC, Götz J. Extracellular Vesicles Containing P301L Mutant Tau
957 Accelerate Pathological Tau Phosphorylation and Oligomer Formation but Do Not Seed
958 Mature Neurofibrillary Tangles in ALZ17 Mice. J Alzheimer's Dis. 2016;

959 42. Polanco JC, Scicluna BJ, Hill AF, Götz J. Extracellular Vesicles Isolated from the Brains of
960 rTg4510 Mice Seed Tau Protein Aggregation in a Threshold-dependent Manner. J Biol
961 Chem [Internet]. 2016 Jun 10 [cited 2018 Mar 18];291(24):12445–66. Available from:
962 http://www.jbc.org/lookup/doi/10.1074/jbc.M115.709485

963 43. Rajendran L, Knobloch M, Geiger KD, Dienel S, Nitsch R, Simons K, et al. Increased Aβ
964 Production Leads to Intracellular Accumulation of Aβ in Flotillin-1-Positive Endosomes.
965 Neurodegener Dis [Internet]. 2007 Jun 29 [cited 2017 Jan 23];4(2–3):164–70. Available
966 from: http://www.ncbi.nlm.nih.gov/pubmed/17596711

967 44. Kapogiannis D, Boxer A, Schwartz JB, Abner EL, Biragyn A, Masharani U, et al.
968 Dysfunctionally phosphorylated type 1 insulin receptor substrate in neural-derived blood
969 exosomes of preclinical Alzheimer's disease. FASEB J [Internet]. 2015;29(2):589–96.
970 Available from: http://www.ncbi.nlm.nih.gov/pubmed/25342129

971 45. Goetzl EJ, Boxer A, Schwartz JB, Abner EL, Petersen RC, Miller BL, et al. Altered lysosomal
972 proteins in neural-derived plasma exosomes in preclinical Alzheimer disease. Neurology
973 [Internet]. 2015;85(1):40–7. Available from:
974 http://www.ncbi.nlm.nih.gov/pubmed/26062630

975 46. Gámez-Valero A, Campdelacreu J, Vilas D, Ispierto L, Reñé R, Álvarez R, et al. Exploratory
976 study on microRNA profiles from plasma-derived extracellular vesicles in Alzheimer's

977 disease and dementia with Lewy bodies. Transl Neurodegener [Internet]. 2019 Oct 3
978 [cited 2020 Oct 16];8(1). Available from: https://pubmed.ncbi.nlm.nih.gov/31592314/
979 47. Li F, Xie XY, Sui XF, Wang P, Chen Z, Zhang JB. Profile of Pathogenic Proteins and
980 MicroRNAs in Plasma-derived Extracellular Vesicles in Alzheimer's Disease: A Pilot Study.
981 Neuroscience. 2020;
982 48. Jia L, Zhu M, Kong C, Pang Y, Zhang H, Qiu Q, et al. Blood neuro-exosomal synaptic
983 proteins predict Alzheimer's disease at the asymptomatic stage. Alzheimer's Dement
984 [Internet]. 2020 [cited 2020 Oct 16]; Available from:
985 https://pubmed.ncbi.nlm.nih.gov/32776690/
986 49. Yuyama K, Sun H, Mitsutake S, Igarashi Y. Sphingolipid-modulated Exosome Secretion
987 Promotes Clearance of Amyloid- by Microglia. J Biol Chem [Internet]. 2012 Mar 30 [cited
988 2017 Jan 23];287(14):10977–89. Available from:
989 http://www.ncbi.nlm.nih.gov/pubmed/22303002
990 50. Yuyama K, Sun H, Sakai S, Mitsutake S, Okada M, Tahara H, et al. Decreased
991 Amyloid- Pathologies by Intracerebral Loading of Glycosphingolipid-enriched Exosomes
992 in Alzheimer Model Mice. J Biol Chem. 2014 Aug;289(35):24488–98.
993 51. An K, Klyubin I, Kim Y, Jung J, Mably AJ, O'Dowd ST, et al. Exosomes neutralize synaptic-
994 plasticity-disrupting activity of Aβ assemblies in vivo. Mol Brain [Internet]. 2013 Nov 13
995 [cited 2017 Jan 23];6(1):47. Available from:
996 http://www.ncbi.nlm.nih.gov/pubmed/24284042
997 52. Dinkins MB, Dasgupta S, Wang G, Zhu G, Bieberich E. Exosome reduction in vivo is
998 associated with lower amyloid plaque load in the 5XFAD mouse model of Alzheimer's

999 disease. Neurobiol Aging [Internet]. 2014 Aug [cited 2017 Jan 23];35(8):1792–800.
1000 Available from: http://linkinghub.elsevier.com/retrieve/pii/S0197458014002048
1001 53. Dinkins MB, Enasko J, Hernandez C, Wang G, Kong J, Helwa I, et al. Neutral
1002 Sphingomyelinase-2 Deficiency Ameliorates Alzheimer's Disease Pathology and Improves
1003 Cognition in the 5XFAD Mouse. J Neurosci [Internet]. 2016 Aug 17 [cited 2017 Jan
1004 23];36(33):8653–67. Available from:
1005 http://www.jneurosci.org/lookup/doi/10.1523/JNEUROSCI.1429-16.2016
1006 54. Cogswell JP, Ward J, Taylor IA, Waters M, Shi Y, Cannon B, et al. Identification of miRNA
1007 changes in Alzheimer's disease brain and CSF yields putative biomarkers and insights into
1008 disease pathways. J Alzheimers Dis [Internet]. 2008;14(1):27–41. Available from:
1009 http://www.ncbi.nlm.nih.gov/entrez/query.fcgi?cmd=Retrieve&db=PubMed&dopt=Citati
1010 on&list_uids=18525125
1011 55. Lau P, Bossers K, Janky R, Salta E, Frigerio CS, Barbash S, et al. Alteration of the microRNA
1012 network during the progression of Alzheimer's disease. EMBO Mol Med. 2013;
1013 56. Wang WX, Huang Q, Hu Y, Stromberg AJ, Nelson PT. Patterns of microRNA expression in
1014 normal and early Alzheimer's disease human temporal cortex: White matter versus gray
1015 matter. Acta Neuropathol. 2011;
1016 57. Cheng L, Doecke JD, Sharples RA, Villemagne VL, Fowler CJ, Rembach A, et al. Prognostic
1017 serum miRNA biomarkers associated with Alzheimer's disease shows concordance with
1018 neuropsychological and neuroimaging assessment. Mol Psychiatry [Internet]. 2015 Oct
1019 28 [cited 2018 Mar 18];20(10):1188–96. Available from:
1020 http://www.nature.com/articles/mp2014127

1021 58. Nikitidou E, Khoonsari PE, Shevchenko G, Ingelsson M, Kultima K, Erlandsson A. Increased
1022 Release of Apolipoprotein E in Extracellular Vesicles Following Amyloid-β Protofibril
1023 Exposure of Neuroglial Co-Cultures. J Alzheimers Dis [Internet]. 2017 Aug 29 [cited 2018
1024 Mar 18];60(1):305–21. Available from:
1025 http://www.medra.org/servlet/aliasResolver?alias=iospress&doi=10.3233/JAD-170278
1026 59. van Niel G, Bergam P, Di Cicco A, Hurbain I, Lo Cicero A, Dingli F, et al. Apolipoprotein E
1027 Regulates Amyloid Formation within Endosomes of Pigment Cells. Cell Rep [Internet].
1028 2015 Oct 6 [cited 2017 Jan 8];13(1):43–51. Available from:
1029 http://www.ncbi.nlm.nih.gov/pubmed/26387950
1030 60. Abdullah M, Takase H, Nunome M, Enomoto H, Ito J, Gong J-S, et al. Amyloid-β Reduces
1031 Exosome Release from Astrocytes by Enhancing JNK Phosphorylation. J Alzheimer's Dis
1032 [Internet]. 2016 Aug 8 [cited 2017 Jan 8];53(4):1433–41. Available from:
1033 http://www.ncbi.nlm.nih.gov/pubmed/27392863
1034 61. Peng KY, Pérez-González R, Alldred MJ, Goulbourne CN, Morales-Corraliza J, Saito M, et
1035 al. Apolipoprotein E4 genotype compromises brain exosome production. Brain. 2019;
1036 62. Yang Y, Keene CD, Peskind ER, Galasko DR, Hu S-C, Cudaback E, et al. Cerebrospinal Fluid
1037 Particles in Alzheimer Disease and Parkinson Disease. J Neuropathol Exp Neurol
1038 [Internet]. 2015 Jul [cited 2017 Jan 8];74(7):672–87. Available from:
1039 http://www.ncbi.nlm.nih.gov/pubmed/26083568
1040 63. Watt B, van Niel G, Raposo G, Marks MS. PMEL: a pigment cell-specific model for
1041 functional amyloid formation. Pigment Cell Melanoma Res [Internet]. 2013 May [cited
1042 2017 Jan 8];26(3):300–15. Available from:

1043 http://www.ncbi.nlm.nih.gov/pubmed/23350640

1044 64. van Niel G. Study of Exosomes Shed New Light on Physiology of Amyloidogenesis. Cell
1045 Mol Neurobiol [Internet]. 2016 Apr 17 [cited 2017 Jan 8];36(3):327–42. Available from:
1046 http://link.springer.com/10.1007/s10571-016-0357-0

1047 65. Zhao F, Zhao T, Deng L, Lv D, Zhang X, Pan X, et al. Visualizing the Essential Role of
1048 Complete Virion Assembly Machinery in Efficient Hepatitis C Virus Cell-to-Cell
1049 Transmission by a Viral Infection-Activated Split-Intein-Mediated Reporter System.
1050 Diamond MS, editor. J Virol [Internet]. 2017 Jan 15 [cited 2018 Mar 18];91(2):e01720-16.
1051 Available from: http://www.ncbi.nlm.nih.gov/pubmed/27852847

1052 66. Li X-F, Wang Y, Zheng D-D, Xu H-X, Wang T, Pan M, et al. M1 macrophages promote
1053 aortic valve calcification mediated by microRNA-214/TWIST1 pathway in valvular
1054 interstitial cells. Am J Transl Res [Internet]. 2016 [cited 2018 Mar 18];8(12):5773–83.
1055 Available from: http://www.ncbi.nlm.nih.gov/pubmed/28078049

1056 67. Gao W, Liu H, Yuan J, Wu C, Huang D, Ma Y, et al. Exosomes derived from mature
1057 dendritic cells increase endothelial inflammation and atherosclerosis *via* membrane TNF-
1058 α mediated NF-κB pathway. J Cell Mol Med [Internet]. 2016 Dec [cited 2018 Mar
1059 18];20(12):2318–27. Available from: http://www.ncbi.nlm.nih.gov/pubmed/27515767

1060 68. Pienimaeki-Roemer A, Kuhlmann K, Böttcher A, Konovalova T, Black A, Orsó E, et al.
1061 Lipidomic and proteomic characterization of platelet extracellular vesicle subfractions
1062 from senescent platelets. Transfusion [Internet]. 2015 Mar [cited 2018 Mar
1063 15];55(3):507–21. Available from: http://www.ncbi.nlm.nih.gov/pubmed/25332113

1064 69. Vella LJ, Scicluna BJ, Cheng L, Bawden EG, Masters CL, Ang C-S, et al. A rigorous method

1065 to enrich for exosomes from brain tissue. J Extracell Vesicles [Internet]. 2017 Jan 26
1066 [cited 2018 Jan 18];6(1):1348885. Available from:
1067 http://www.ncbi.nlm.nih.gov/pubmed/28804598
1068 70. Huang Y, Cheng L, Turchinovich A, Mahairaki V, Troncoso JC, Pletniková O, et al. Influence
1069 of species and processing parameters on recovery and content of brain tissue-derived
1070 extracellular vesicles. J Extracell Vesicles. 2020;
1071 71. Lotvall J, Hill AF, Hochberg F, Buzas EI, Di Vizio D, Gardiner C, et al. Minimal experimental
1072 requirements for definition of extracellular vesicles and their functions: a position
1073 statement from the International Society for Extracellular Vesicles. J Extracell Vesicles
1074 [Internet]. 2014;3:26913. Available from:
1075 http://www.ncbi.nlm.nih.gov/pubmed/25536934
1076 72. Witwer KW, Soekmadji C, Hill AF, Wauben MH, Buzas EI, Di Vizio D, et al. Updating the
1077 MISEV minimal requirements for extracellular vesicle studies: building bridges to
1078 reproducibility. J Extracell Vesicles. 2017;
1079 73. Van Deun J, Mestdagh P, Agostinis P, Akay Ö, Anand S, Anckaert J, et al. EV-TRACK:
1080 Transparent reporting and centralizing knowledge in extracellular vesicle research. Nat
1081 Methods. 2017;14(3).
1082 74. Braak H, Braak E. Neuropathological stageing of Alzheimer-related changes. Vol. 82, Acta
1083 Neuropathologica. Springer-Verlag; 1991. p. 239–59.
1084 75. Mirra SS, Heyman A, McKeel D, Sumi SM, Crain BJ, Brownlee LM, et al. The consortium to
1085 establish a registry for Alzheimer's disease (CERAD). Part II. Standardization of the
1086 neuropathologic assessment of Alzheimer's disease. Neurology. 1991;41(4):479–86.

1087 76. Morris JC, Heyman A, Mohs RC, Hughes JP, van Belle G, Fillenbaum G, et al. The
1088 consortium to establish a registry for alzheimer's disease (CERAD). Part I. Clinical and
1089 neuropsychological assessment of alzheimer's disease. Neurology. 1989;39(9):1159–65.
1090 77. Hixson JE, Vernier DT. Restriction isotyping of human apolipoprotein E by gene
1091 amplification and cleavage with HhaI - PubMed. J Lipid Res. 1990;31(3):545–8.
1092 78. Cheng L, Hill AF. Small RNA library construction for exosomal RNA from biological
1093 samples for the ion torrent PGM™ and ion S5™ system. In: Methods in Molecular
1094 Biology. 2017.
1095 79. Roberts A, Pachter L. Streaming fragment assignment for real-time analysis of
1096 sequencing experiments. Nat Methods. 2013 Jan;10(1):71–3.
1097 80. Anders S, Huber W. Differential expression analysis for sequence count data. Genome
1098 Biol. 2010 Oct;11(10).
1099 81. Love MI, Huber W, Anders S. Moderated estimation of fold change and dispersion for
1100 RNA-seq data with DESeq2. Genome Biol [Internet]. 2014 Dec 5 [cited 2014 Dec
1101 23];15(12):550. Available from:
1102 http://www.pubmedcentral.nih.gov/articlerender.fcgi?artid=4302049&tool=pmcentrez&
1103 rendertype=abstract
1104 82. Szklarczyk D, Gable AL, Lyon D, Junge A, Wyder S, Huerta-Cepas J, et al. STRING v11:
1105 Protein-protein association networks with increased coverage, supporting functional
1106 discovery in genome-wide experimental datasets. Nucleic Acids Res. 2019
1107 Jan;47(D1):D607–13.
1108 83. Kanehisa M, Goto S. KEGG: Kyoto Encyclopedia of Genes and Genomes. Vol. 28, Nucleic

1109 Acids Research. Oxford University Press; 2000. p. 27–30.

1110 84. Nolte-'t Hoen EN, Buermans HP, Waasdorp M, Stoorvogel W, Wauben MH, t Hoen PA.
1111 Deep sequencing of RNA from immune cell-derived vesicles uncovers the selective
1112 incorporation of small non-coding RNA biotypes with potential regulatory functions.
1113 Nucleic Acids Res [Internet]. 2012/07/24. 2012; Available from:
1114 http://www.ncbi.nlm.nih.gov/pubmed/22821563

1115 85. Tosar JP, Gambaro F, Sanguinetti J, Bonilla B, Witwer KW, Cayota A. Assessment of small
1116 RNA sorting into different extracellular fractions revealed by high-throughput sequencing
1117 of breast cell lines. Nucleic Acids Res [Internet]. 2015;43(11):5601–16. Available from:
1118 http://www.ncbi.nlm.nih.gov/pubmed/25940616

1119 86. Driedonks TAP, van der Grein SG, Ariyurek Y, Buermans HPJ, Jekel H, Chow FWN, et al.
1120 Immune stimuli shape the small non-coding transcriptome of extracellular vesicles
1121 released by dendritic cells. Cell Mol Life Sci. 2018;

1122 87. Jeppesen DK, Fenix AM, Franklin JL, Higginbotham JN, Zhang Q, Zimmerman LJ, et al.
1123 Reassessment of Exosome Composition. Cell. 2019;

1124 88. Chiou NT, Kageyama R, Ansel KM. Selective Export into Extracellular Vesicles and
1125 Function of tRNA Fragments during T Cell Activation. Cell Rep. 2018 Dec 18;25(12):3356-
1126 3370.e4.

1127 89. Nabet BY, Qiu Y, Shabason JE, Wu TJ, Yoon T, Kim BC, et al. Exosome RNA Unshielding
1128 Couples Stromal Activation to Pattern Recognition Receptor Signaling in Cancer. Cell.
1129 2017 Jul 13;170(2):352-366.e13.

1130 90. Haderk F, Schulz R, Iskar M, Cid LL, Worst T, Willmund K V., et al. Tumor-derived

1131 exosomes modulate PD-L1 expression in monocytes. Sci Immunol [Internet]. 2017 Jul 28
1132 [cited 2020 Mar 6];2(13). Available from:
1133 http://www.ncbi.nlm.nih.gov/pubmed/28754746
1134 91. Muraoka S, Lin W, Chen M, Hersh SW, Emili A, Xia W, et al. Assessment of separation
1135 methods for extracellular vesicles from human and mouse brain tissues and human
1136 cerebrospinal fluids. Methods. 2020;
1137 92. Gallart-Palau X, Guo X, Serra A, Sze SK. Alzheimer's disease progression characterized by
1138 alterations in the molecular profiles and biogenesis of brain extracellular vesicles.
1139 Alzheimer's Res Ther. 2020;
1140 93. Cataldo AM, Peterhoff CM, Troncoso JC, Gomez-Isla T, Hyman BT, Nixon RA. Endocytic
1141 pathway abnormalities precede amyloid beta deposition in sporadic Alzheimer's disease
1142 and Down syndrome: differential effects of APOE genotype and presenilin mutations. Am
1143 J Pathol [Internet]. 2000 Jul [cited 2017 Jan 30];157(1):277–86. Available from:
1144 http://www.ncbi.nlm.nih.gov/pubmed/10880397
1145 94. Caselli RJ, Reiman EM, Locke DEC, Hutton ML, Hentz JG, Hoffman-Snyder C, et al.
1146 Cognitive domain decline in healthy apolipoprotein E ε4 homozygotes before the
1147 diagnosis of mild cognitive impairment. Arch Neurol. 2007;
1148 95. Magill ST, Cambronne XA, Luikart BW, Lioy DT, Leighton BH, Westbrook GL, et al.
1149 MicroRNA-132 regulates dendritic growth and arborization of newborn neurons in the
1150 adult hippocampus. Proc Natl Acad Sci U S A. 2010;
1151 96. Luikart BW, Bensen ASL, Washburn EK, Perederiy J V., Su KG, Li Y, et al. MiR-132 mediates
1152 the integration of newborn neurons into the adult dentate gyrus. PLoS One. 2011;

1153 97. Vo N, Klein ME, Varlamova O, Keller DM, Yamamoto T, Goodman RH, et al. A cAMP-
1154 response element binding protein-induced microRNA regulates neuronal morphogenesis.
1155 Proc Natl Acad Sci U S A. 2005;
1156 98. Smith PY, Hernandez-Rapp J, Jolivette F, Lecours C, Bisht K, Goupil C, et al. MiR-132/212
1157 deficiency impairs tau metabolism and promotes pathological aggregation in vivo. Hum
1158 Mol Genet. 2015;
1159 99. Hernandez-Rapp J, Smith PY, Filali M, Goupil C, Planel E, Magill ST, et al. Memory
1160 formation and retention are affected in adult miR-132/212 knockout mice. Behav Brain
1161 Res. 2015;
1162 100. Faghihi MA, Zhang M, Huang J, Modarresi F, Van der Brug MP, Nalls MA, et al. Evidence
1163 for natural antisense transcript-mediated inhibition of microRNA function. Genome Biol.
1164 2010;
1165 101. Qian Q, Zhang J, He FP, Bao WX, Zheng TT, Zhou DM, et al. Down-regulated expression of
1166 microRNA-338-5p contributes to neuropathology in Alzheimer's disease. FASEB J. 2019;
1167 102. Hampel H, Vassar R, De Strooper B, Hardy J, Willem M, Singh N, et al. The β-Secretase
1168 BACE1 in Alzheimer's Disease. Biological Psychiatry. 2020.
1169 103. Sharma N, Kumawat KL, Rastogi M, Basu A, Singh SK. Japanese Encephalitis Virus exploits
1170 the microRNA-432 to regulate the expression of Suppressor of Cytokine Signaling (SOCS)
1171 5. Sci Rep. 2016;
1172 104. Zeng Z, Liu Y, Zheng W, Liu L, Yin H, Zhang S, et al. MicroRNA-129-5p alleviates nerve
1173 injury and inflammatory response of Alzheimer's disease via downregulating SOX6. Cell
1174 Cycle. 2019;

1175 105. Zongaro S, Hukema R, D'antoni S, Davidovic L, Barbry P, Catania MV, et al. The 3' UTR of
1176 FMR1 mRNA is a target of miR-101, miR-129-5p and miR-221: Implications for the
1177 molecular pathology of FXTAS at the synapse. Hum Mol Genet. 2013;
1178 106. Wu C, Zhang X, Chen P, Ruan X, Liu W, Li Y, et al. MicroRNA-129 modulates neuronal
1179 migration by targeting Fmr1 in the developing mouse cortex. Cell Death Dis. 2019;
1180 107. Cheng L, Vella LJ, Barnham KJ, McLean C, Masters CL, Hill AF. Small RNA fingerprinting of
1181 Alzheimer's disease frontal cortex extracellular vesiclesand their comparison with
1182 peripheral extracellular vesicles. J Extracell Vesicles. 2020;
1183 108. Marty V, Labialle S, Bortolin-Cavaillé ML, De Medeiros GF, Moisan MP, Florian C, et al.
1184 Deletion of the miR-379/miR-410 gene cluster at the imprinted Dlk1-Dio3 locus enhances
1185 anxiety-related behaviour. Hum Mol Genet. 2016;
1186 109. Sabirzhanov B, Zhao Z, Stoica BA, Loane DJ, Wu J, Borroto C, et al. Downregulation of
1187 miR-23a and miR-27a following experimental traumatic brain injury induces neuronal cell
1188 death through activation of proapoptotic Bcl-2 proteins. J Neurosci. 2014;
1189 110. Han K, Gennarino VA, Lee Y, Pang K, Hashimoto-Torii K, Choufani S, et al. Human-specific
1190 regulation of MeCP2 levels in fetal brains by microRNA miR-483-5p. Genes Dev. 2013;
1191 111. Bellingham SA, Coleman BM, Hill AF. Small RNA deep sequencing reveals a distinct
1192 miRNA signature released in exosomes from prion-infected neuronal cells. Nucleic Acids
1193 Res [Internet]. 2012/09/12. 2012;40(21):10937–49. Available from:
1194 http://www.ncbi.nlm.nih.gov/pubmed/22965126
1195 112. Vojtech L, Woo S, Hughes S, Levy C, Ballweber L, Sauteraud RP, et al. Exosomes in human
1196 semen carry a distinctive repertoire of small non-coding RNAs with potential regulatory

1197 functions. Nucleic Acids Res [Internet]. 2014 Jun 17 [cited 2018 Sep 8];42(11):7290–304.
1198 Available from: https://academic.oup.com/nar/article-lookup/doi/10.1093/nar/gku347
1199 113. Godoy PM, Bhakta NR, Barczak AJ, Cakmak H, Fisher S, MacKenzie TC, et al. Large
1200 Differences in Small RNA Composition Between Human Biofluids. Cell Rep. 2018;
1201 114. Torres AG, Batlle E, Ribas de Pouplana L. Role of tRNA modifications in human diseases.
1202 Trends in Molecular Medicine. 2014.
1203 115. Kirchner S, Ignatova Z. Emerging roles of tRNA in adaptive translation, signalling
1204 dynamics and disease [Internet]. Vol. 16, Nature Reviews Genetics. Nature Publishing
1205 Group; 2015 [cited 2020 Oct 27]. p. 98–112. Available from:
1206 https://www.nature.com/articles/nrg3861
1207 116. Goodarzi H, Nguyen HCB, Zhang S, Dill BD, Molina H, Tavazoie SF. Modulated expression
1208 of specific tRNAs drives gene expression and cancer progression. Cell. 2016;
1209 117. Gámbaro F, Li Calzi M, Fagúndez P, Costa B, Greif G, Mallick E, et al. Stable tRNA halves
1210 can be sorted into extracellular vesicles and delivered to recipient cells in a
1211 concentration-dependent manner. RNA Biol [Internet]. 2019 [cited 2020 Jun 23];
1212 Available from: https://pubmed.ncbi.nlm.nih.gov/31885318/
1213 118. Driedonks TAP, Nolte-T'Hoen ENM. Circulating Y-RNAs in extracellular vesicles and
1214 ribonucleoprotein complexes; Implications for the immune system [Internet]. Vol. 10,
1215 Frontiers in Immunology. Frontiers Media S.A.; 2019 [cited 2020 Jun 23]. Available from:
1216 https://pubmed.ncbi.nlm.nih.gov/30697216/
1217 119. Boccitto M, Wolin SL. Ro60 and Y RNAs: structure, functions, and roles in autoimmunity
1218 [Internet]. Vol. 54, Critical Reviews in Biochemistry and Molecular Biology. Taylor and

1219 Francis Ltd; 2019 [cited 2020 Jun 23]. p. 133–52. Available from:
1220 https://pubmed.ncbi.nlm.nih.gov/31084369/
1221 120. Scheckel C, Drapeau E, Frias MA, Park CY, Fak J, Zucker-Scharff I, et al. Regulatory
1222 consequences of neuronal ELAV-like protein binding to coding and non-coding RNAs in
1223 human brain. Elife. 2016;
1224 121. Matera AG, Wang Z. A day in the life of the spliceosome. Nature Reviews Molecular Cell
1225 Biology. 2014.
1226 122. Bai B, Hales CM, Chen PC, Gozal Y, Dammer EB, Fritz JJ, et al. U1 small nuclear
1227 ribonucleoprotein complex and RNA splicing alterations in Alzheimer's disease. Proc Natl
1228 Acad Sci U S A. 2013;
1229 123. Hales CM, Dammer EB, Diner I, Yi H, Seyfried NT, Gearing M, et al. Aggregates of Small
1230 Nuclear Ribonucleic Acids (snRNAs) in Alzheimer's Disease. Brain Pathol. 2014;
1231 124. Brunello CA, Merezhko M, Uronen RL, Huttunen HJ. Mechanisms of secretion and
1232 spreading of pathological tau protein. Cellular and Molecular Life Sciences. 2020.
1233 125. Baker S, Polanco JC, Götz J. Extracellular Vesicles Containing P301L Mutant Tau
1234 Accelerate Pathological Tau Phosphorylation and Oligomer Formation but Do Not Seed
1235 Mature Neurofibrillary Tangles in ALZ17 Mice. Gozes I, editor. J Alzheimer's Dis
1236 [Internet]. 2016 Oct 4 [cited 2018 Mar 18];54(3):1207–17. Available from:
1237 http://www.medra.org/servlet/aliasResolver?alias=iospress&doi=10.3233/JAD-160371
1238 126. DeLeo AM, Ikezu T. Extracellular Vesicle Biology in Alzheimer's Disease and Related
1239 Tauopathy. Journal of Neuroimmune Pharmacology. 2018.
1240 127. Liu S, Mahairaki V, Bai H, Ding Z, Li J, Witwer KW, et al. Highly Purified Human

1241 Extracellular Vesicles Produced by Stem Cells Alleviate Aging Cellular Phenotypes of
1242 Senescent Human Cells. Stem Cells. 2019;
1243 128. The Role of Interleukin-18, Oxidative Stress and Metabolic Syndrome in Alzheimer's
1244 Disease. J Clin Med. 2017;
1245 129. Krapfenbauer K, Engidawork E, Cairns N, Fountoulakis M, Lubec G. Aberrant expression
1246 of peroxiredoxin subtypes in neurodegenerative disorders. Brain Res. 2003;
1247 130. Lee YJ, Goo JS, Kim JE, Nam SH, Hwang IS, Choi S Il, et al. Peroxiredoxin I regulates the
1248 component expression of γ-secretase complex causing the Alzheimer's disease. Lab Anim
1249 Res. 2011;
1250 131. Mullen L, Hanschmann EM, Lillig CH, Herzenberg LA, Ghezzi P. Cysteine oxidation targets
1251 peroxiredoxins 1 and 2 for exosomal release through a novel mechanism of Redox-
1252 dependent secretion. Mol Med. 2015;
1253 132. Szabó-Taylor K, Tóth E, Balogh AM, Sódar BW, Kádár L, Pálóczi K, et al. Monocyte
1254 activation drives preservation of membrane thiols by promoting release of oxidised
1255 membrane moieties via extracellular vesicles. Free Radic Biol Med. 2017;
1256 133. Sekito A, Koide-Yoshida S, Niki T, Taira T, Iguchi-Ariga SMM, Ariga H. DJ-1 interacts with
1257 HIPK1 and affects H2O2-induced cell death. Free Radic Res. 2006;
1258 134. Junn E, Jang WH, Zhao X, Jeong BS, Mouradian MM. Mitochondrial localization of DJ-1
1259 leads to enhanced neuroprotection. J Neurosci Res. 2009;
1260 135. Hauptmann S, Scherping I, Dröse S, Brandt U, Schulz KL, Jendrach M, et al. Mitochondrial
1261 dysfunction: An early event in Alzheimer pathology accumulates with age in AD
1262 transgenic mice. Neurobiol Aging. 2009;

1263 136. Leuner K, Hauptmann S, Abdel-Kader R, Scherping I, Keil U, Strosznajder JB, et al.
1264 Mitochondrial dysfunction: The first domino in brain aging and Alzheimer's disease?
1265 Antioxidants and Redox Signaling. 2007.
1266 137. Müller WE, Eckert A, Kurz C, Eckert GP, Leuner K. Mitochondrial dysfunction: Common
1267 final pathway in brain aging and alzheimer's disease-therapeutic aspects. In: Molecular
1268 Neurobiology. 2010.
1269 138. Cadonic C, Sabbir MG, Albensi BC. Mechanisms of Mitochondrial Dysfunction in
1270 Alzheimer's Disease. Molecular Neurobiology. 2016.
1271 139. Yamanaka K, Sasagawa Y, Ogura T. Recent advances in p97/VCP/Cdc48 cellular functions.
1272 Biochimica et Biophysica Acta - Molecular Cell Research. 2012.
1273 140. Guo X, Sun X, Hu D, Wang YJ, Fujioka H, Vyas R, et al. VCP recruitment to mitochondria
1274 causes mitophagy impairment and neurodegeneration in models of Huntington's
1275 disease. Nat Commun. 2016;
1276 141. Zahid S, Oellerich M, Asif AR, Ahmed N. Differential expression of proteins in brain
1277 regions of alzheimer's disease patients. Neurochem Res. 2014;
1278 142. Chen Z, Zhong C. Decoding Alzheimer's disease from perturbed cerebral glucose
1279 metabolism: Implications for diagnostic and therapeutic strategies. Progress in
1280 Neurobiology. 2013.
1281 143. Gibson GE, Sheu KR, Blass JP, Baker A, Carlson KC, Harding B, et al. Reduced Activities of
1282 Thiamine-Dependent Enzymes in the Brains and Peripheral Tissues of Patients with
1283 Alzheimer's Disease. Arch Neurol. 1988;
1284 144. Petrak J, Ivanek R, Toman O, Cmejla R, Cmejlova J, Vyoral D, et al. Déjà vu in proteomics.

1285 A hit parade of repeatedly identified differentially expressed proteins. Proteomics. 2008.
1286 145. Butterfield DA, Lange MLB. Multifunctional roles of enolase in Alzheimer's disease brain:
1287 Beyond altered glucose metabolism. Journal of Neurochemistry. 2009.
1288 146. Funari VA, Crandall JE, Tolan DR. Fructose metabolism in the cerebellum. Cerebellum.
1289 2007.
1290 147. Li B, Yamamori H, Tatebayashi Y, Shafit-Zagardo B, Tanimukai H, Chen S, et al. Failure of
1291 neuronal maturation in Alzheimer disease dentate gyrus. J Neuropathol Exp Neurol.
1292 2008;
1293 148. Boldrini M, Fulmore CA, Tartt AN, Simeon LR, Pavlova I, Poposka V, et al. Human
1294 Hippocampal Neurogenesis Persists throughout Aging. Cell Stem Cell. 2018;
1295 149. Choi ML, Gandhi S. Crucial role of protein oligomerization in the pathogenesis of
1296 Alzheimer's and Parkinson's diseases. FEBS Journal. 2018.
1297 150. Demars M, Hu YS, Gadadhar A, Lazarov O. Impaired neurogenesis is an early event in the
1298 etiology of familial Alzheimer's disease in transgenic mice. J Neurosci Res. 2010;
1299 151. Berg D, Holzmann C, Riess O. 14-3-3 proteins in the nervous system. Nat Rev Neurosci.
1300 2003;
1301 152. Boston PF, Jackson P, Thompson RJ. Human 14-3-3 Protein: Radioimmunoassay, Tissue
1302 Distribution, and Cerebrospinal Fluid Levels in Patients with Neurological Disorders. J
1303 Neurochem. 1982;
1304 153. Baxter HC, Fraser JR, Liu WG, Forster JL, Clokie S, Steinacker P, et al. Specific 14-3-3
1305 isoform detection and immunolocalization in prion diseases. In: Biochemical Society
1306 Transactions. 2002.

1307 154. Toyo-Oka K, Wachi T, Hunt RF, Baraban SC, Taya S, Ramshaw H, et al. 14-3-3ε and ζ
1308 regulate neurogenesis and differentiation of neuronal progenitor cells in the developing
1309 brain. J Neurosci. 2014;
1310 155. Gennarini G, Bizzoca A, Picocci S, Puzzo D, Corsi P, Furley AJW. The role of Gpi-anchored
1311 axonal glycoproteins in neural development and neurological disorders. Molecular and
1312 Cellular Neuroscience. 2017.
1313 156. Gulisano W, Bizzoca A, Gennarini G, Palmeri A, Puzzo D. Role of the adhesion molecule
1314 F3/Contactin in synaptic plasticity and memory. Molecular and Cellular Neuroscience.
1315 2017.
1316 157. Ebel J, Beuter S, Wuchter J, Kriebel M, Volkmer H. Organisation and control of neuronal
1317 connectivity and myelination by cell adhesion molecule neurofascin. Advances in
1318 neurobiology. 2014.
1319 158. Sherman DL, Tait S, Melrose S, Johnson R, Zonta B, Court FA, et al. Neurofascins are
1320 required to establish axonal domains for saltatory conduction. Neuron. 2005;
1321 159. Hattori T, Takei N, Mizuno Y, Kato K, Kohsaka S. Neurotrophic and neuroprotective
1322 effects of neuron-specific enolase on cultured neurons from embryonic rat brain.
1323 Neurosci Res. 1995;
1324 160. Hafner A, Obermajer N, Kos J. γ-Enolase C-terminal peptide promotes cell survival and
1325 neurite outgrowth by activation of the PI3K/Akt and MAPK/ERK signalling pathways.
1326 Biochem J. 2012;
1327 161. Hafner A, Glavan G, Obermajer N, Živin M, Schliebs R, Kos J. Neuroprotective role of γ-
1328 enolase in microglia in a mouse model of Alzheimer's disease is regulated by cathepsin X.

1329 Aging Cell. 2013;

1330 162. Hockfield S, Kalb RG, Zaremba S, Fryer H. Expression of neural proteoglycans correlates

1331 with the acquisition of mature neuronal properties in the mammalian brain. In: Cold

1332 Spring Harbor Symposia on Quantitative Biology. 1990.

1333 163. Bandtlow CE, Zimmermann DR. Proteoglycans in the developing brain: New conceptual

1334 insights for old proteins. Physiological Reviews. 2000.

1335 164. Frischknecht R, Seidenbecher CI. Brevican: A key proteoglycan in the perisynaptic

1336 extracellular matrix of the brain. International Journal of Biochemistry and Cell Biology.

1337 2012.

1338

Figure 1

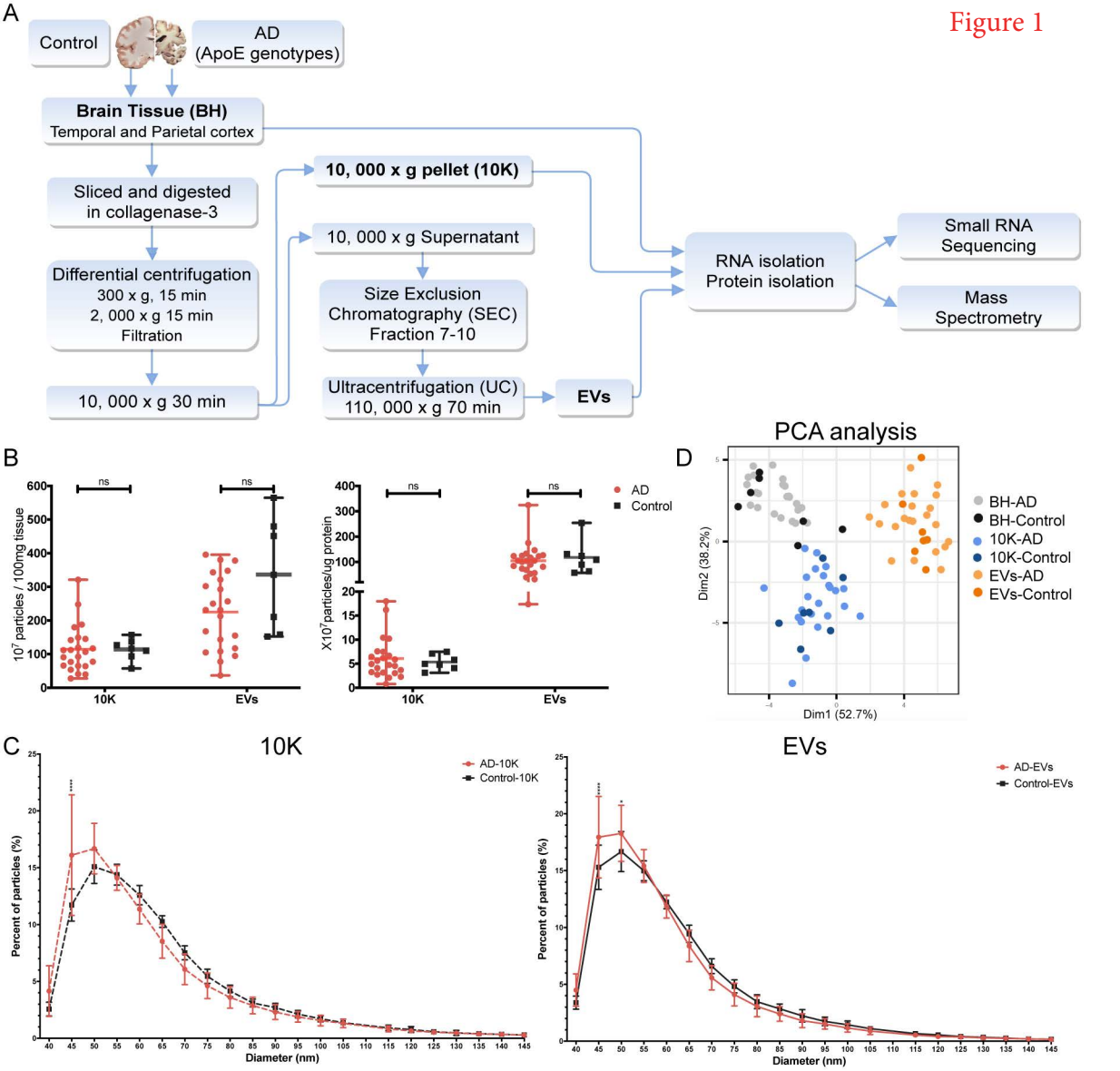
A
Control
AD
(ApoE genotypes)
Brain Tissue (BH)
Temporal and Parietal cortex
Sliced and digested
in collagenase-3
Differential centrifugation
300 x g, 15 min
2, 000 x g 15 min
Filtration
10, 000 x g 30 min
10, 000 x g pellet (10K)
10, 000 x g Supernatant
Size Exclusion
Chromatography (SEC)
Fraction 7-10
Ultracentrifugation (UC)
110, 000 x g 70 min
EVs
RNA isolation
Protein isolation
Small RNA
Sequencing
Mass
Spectrometry
B
ns
10^7 particles / 100mg tissue
X10^7 particles/ug protein
10K
EVs
AD
Control
PCA analysis
D
BH-AD
BH-Control
10K-AD
10K-Control
EVs-AD
EVs-Control
Dim1 (52.7%)
Dim2 (38.2%)
C
10K
AD-10K
Control-10K
EVs
AD-EVs
Control-EVs
Percent of particles (%)
Diameter (nm)

Figure 2

A

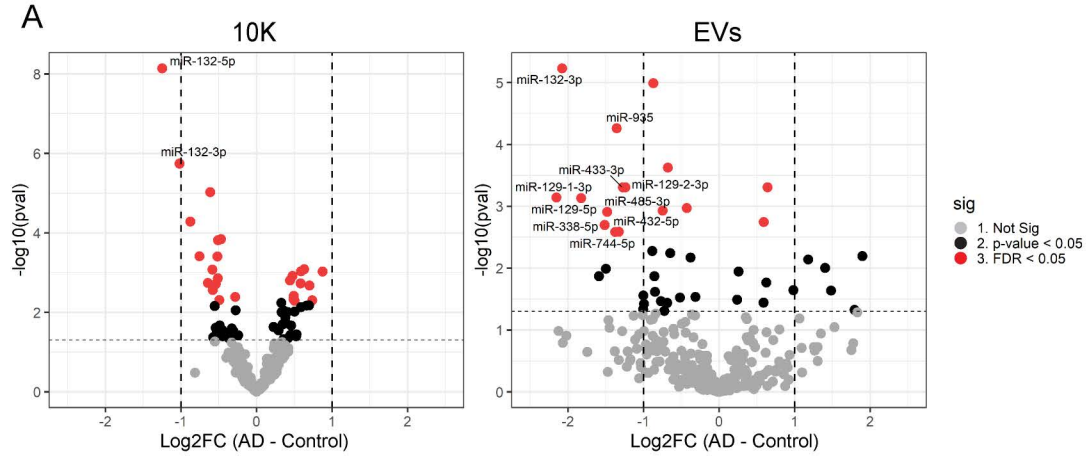


B

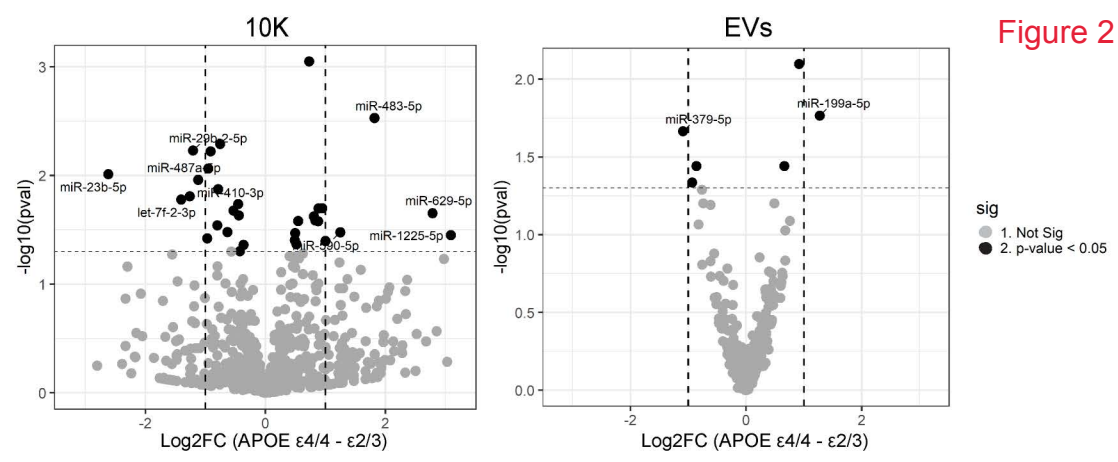


C

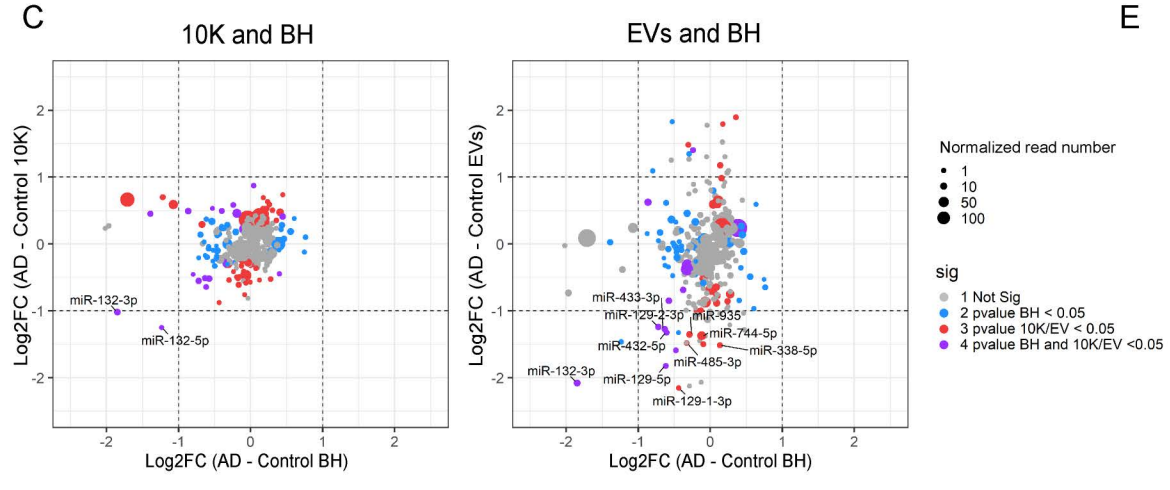


E

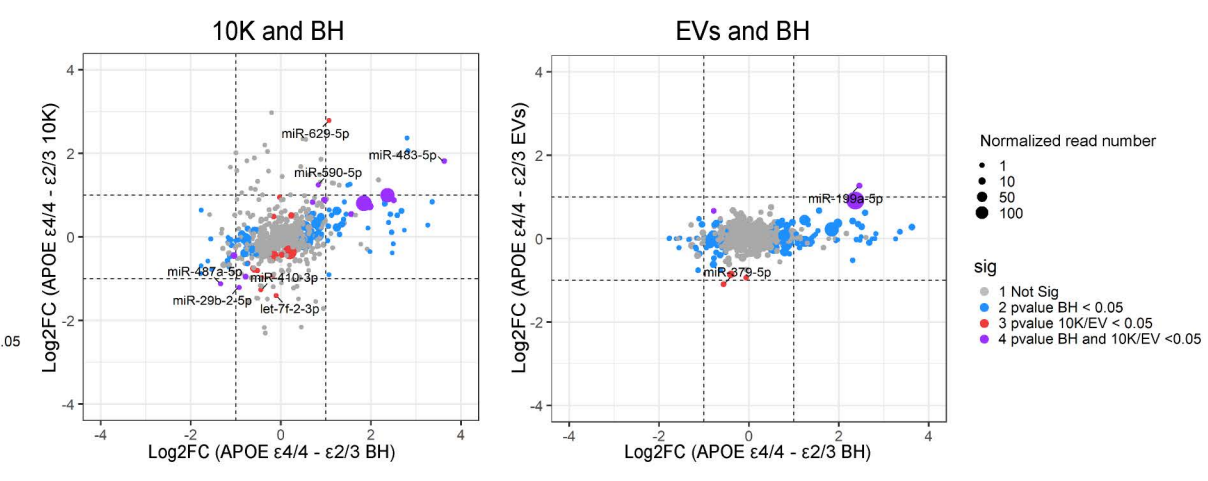


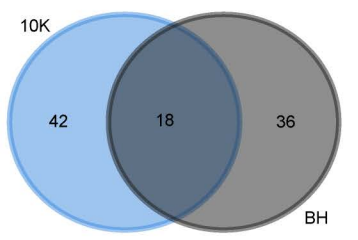


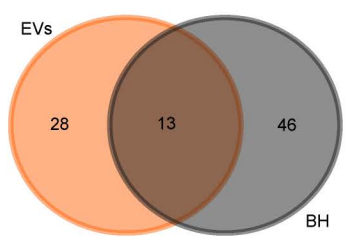


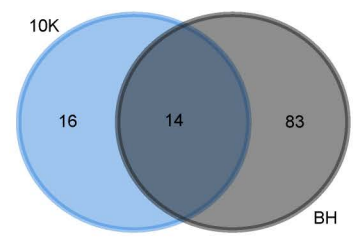


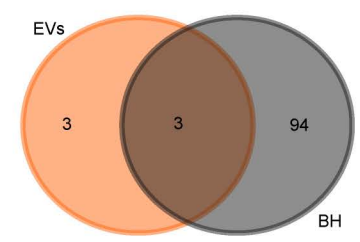


D

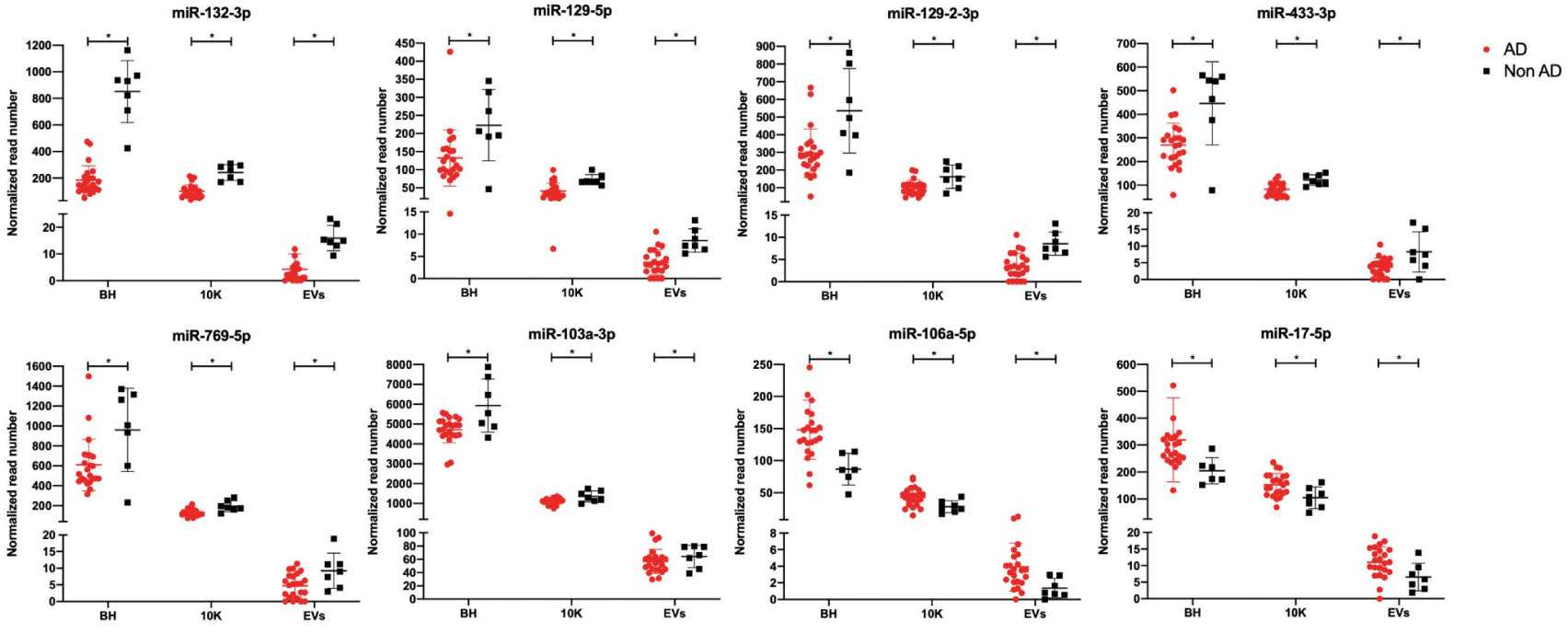


F

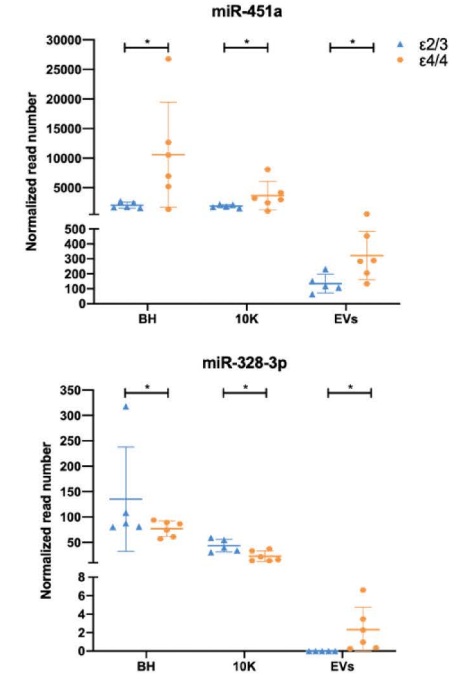

Figure 3

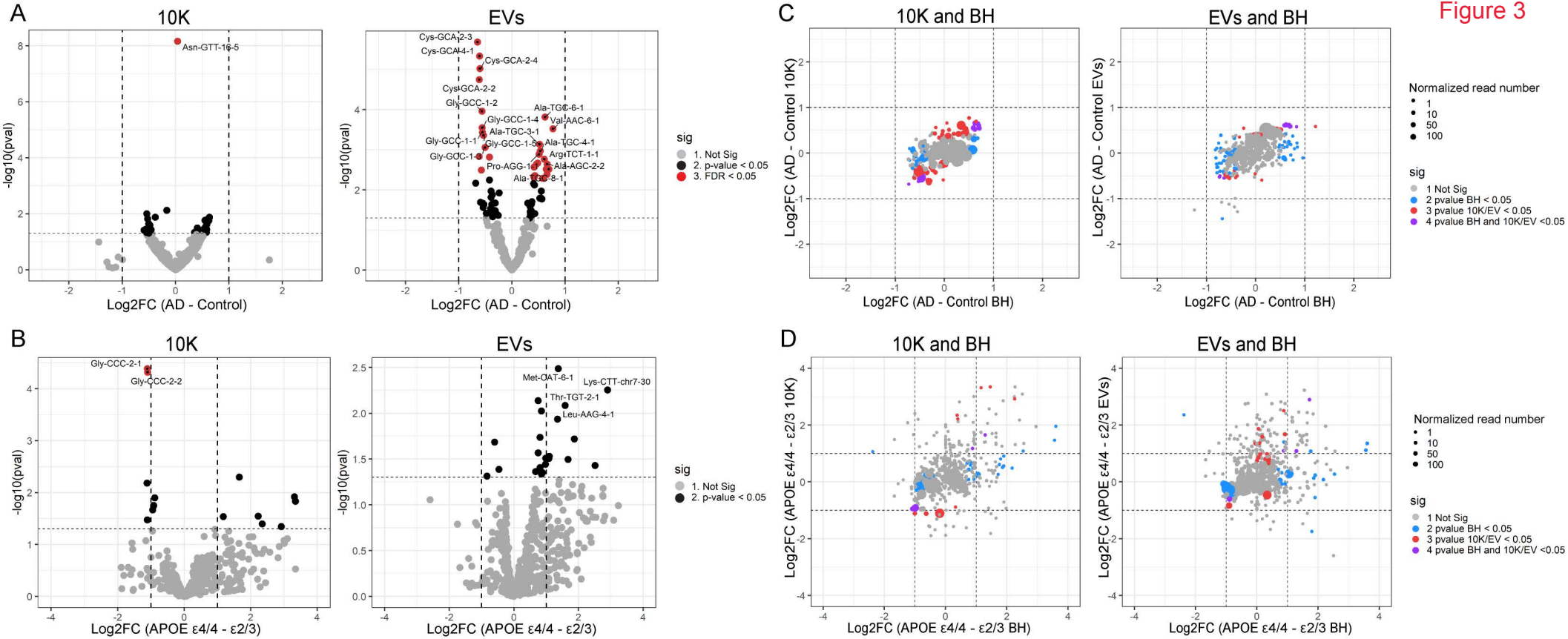
A
10K
EVs
Asn-GTT-16-5
Cys-GCA-2-3
Cys-GCA-4-1
Cys-GCA-2-4
Cys-GCA-2-2
Gly-GCC-1-2
Ala-TGC-6-1
Gly-GCC-1-4
Val-AAC-6-1
Ala-TGC-3-1
Gly-GCC-1-1
Gly-GCC-1-5
Ala-TGC-4-1
Gly-GCC-1-3
Arg-TCT-1-1
Pro-AGG-1-1
Ala-AGC-2-2
Ala-TGC-8-1
-log10(pval)
Log2FC (AD - Control)
sig
1. Not Sig
2. p-value < 0.05
3. FDR < 0.05
B
10K
EVs
Gly-CCC-2-1
Gly-CCC-2-2
Met-CAT-6-1
Lys-CTT-chr7-30
Thr-TGT-2-1
Leu-AAG-4-1
-log10(pval)
Log2FC (APOE ε4/4 - ε2/3)
sig
1. Not Sig
2. p-value < 0.05
C
10K and BH
EVs and BH
Log2FC (AD - Control 10K)
Log2FC (AD - Control EVs)
Log2FC (AD - Control BH)
Normalized read number
1
10
50
100
sig
1 Not Sig
2 pvalue BH < 0.05
3 pvalue 10K/EV < 0.05
4 pvalue BH and 10K/EV <0.05
D
10K and BH
EVs and BH
Log2FC (APOE ε4/4 - ε2/3 10K)
Log2FC (APOE ε4/4 - ε2/3 EVs)
Log2FC (APOE ε4/4 - ε2/3 BH)
Normalized read number
1
10
50
100
sig
1 Not Sig
2 pvalue BH < 0.05
3 pvalue 10K/EV < 0.05
4 pvalue BH and 10K/EV <0.05

Figure 4

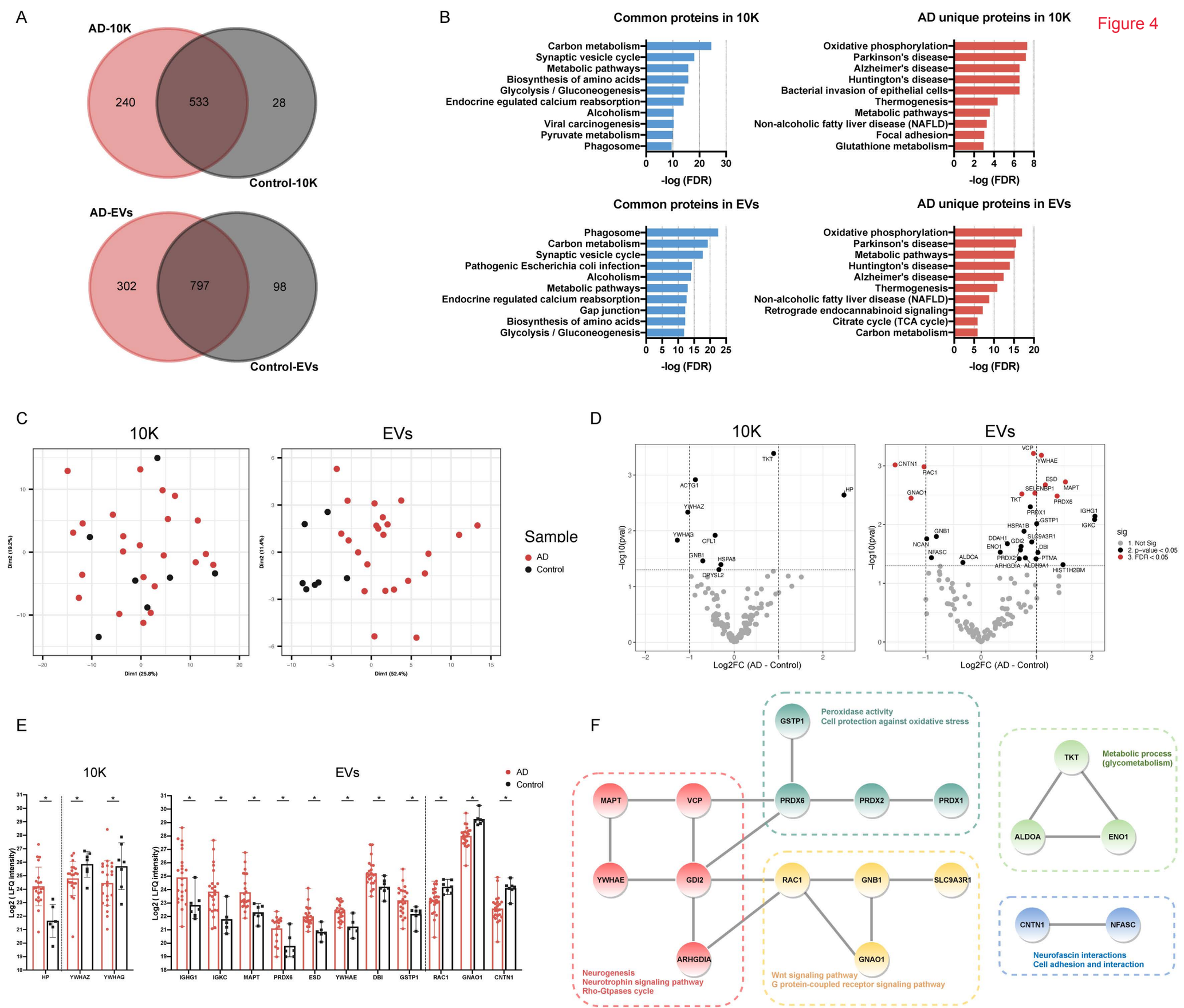
A
AD-10K
240
533
28
Control-10K
AD-EVs
302
797
98
Control-EVs
B
Common proteins in 10K
Carbon metabolism
Synaptic vesicle cycle
Metabolic pathways
Biosynthesis of amino acids
Glycolysis / Gluconeogenesis
Endocrine egulated calcium reabsorption
Alcoholism
Viral carcinogenesis
Pyruvate metabolism
Phagosome
-log (FDR)
AD unique proteins in 10K
Oxidative phosphorylation
Parkinson's disease
Alzheimer's disease
Huntington's disease
Bacterial invasion of epithelial cells
Thermogenesis
Metabolic pathways
Non-alcoholic fatty liver disease (NAFLD)
Focal adhesion
Glutathione metabolism
-log (FDR)
Common proteins in EVs
Phagosome
Carbon metabolism
Synaptic vesicle cycle
Pathogenic Escherichia coli infection
Alcoholism
Metabolic pathways
Endocrine regulated calcium reabsorption
Gap junction
Biosynthesis of amino acids
Glycolysis / Gluconeogenesis
-log (FDR)
AD unique proteins in EVs
Oxidative phosphorylation
Parkinson's disease
Metabolic pathways
Huntington's disease
Alzheimer's disease
Thermogenesis
Non-alcoholic fatty liver disease (NAFLD)
Retrograde endocannabinoid signaling
Citrate cycle (TCA cycle)
Carbon metabolism
-log (FDR)
C
10K
EVs
Dim1 (25.8%)
Dim2 (19.2%)
Dim1 (52.4%)
Dim2 (11.4%)
Sample
AD
Control
D
10K
EVs
TKT
ACTG1
HP
YWHAZ
YWHAG
CFL1
GNB1
HSPA8
DBYSL2
CNTN1
RAC1
GNAO1
VCP
YWHAE
ESD
MAPT
SELENBP1
PRDX6
PRDX1
GSTP1
IGHG1
IGKC
HSPA1B
SLC9A3R1
DDAH1
GDI2
ENO1
DBI
NCAN
NFASC
ALDOA
PRDX2
PTMA
ARHGDIA
ALDH9A1
HIST1H2BM
−log10(pval)
Log2FC (AD - Control)
sig
1. Not Sig
2. p−value < 0.05
3. FDR < 0.05
E
10K
EVs
AD
Control
Log2 ( LFQ intensity)
HP
YWHAZ
YWHAG
IGHG1
IGKC
MAPT
PRDX6
ESD
YWHAE
DBI
GSTP1
RAC1
GNAO1
CNTN1
F
Peroxidase activity
Cell protection against oxidative stress
GSTP1
MAPT
VCP
PRDX6
PRDX2
PRDX1
YWHAE
GDI2
RAC1
GNB1
SLC9A3R1
ARHGDIA
GNAO1
Neurogenesis
Neurotrophin signaling pathway
Rho-Gtpases cycle
Wnt signaling pathway
G protein-coupled receptor signaling pathway
Metabolic process
(glycometabolism)
TKT
ALDOA
ENO1
CNTN1
NFASC
Neurofascin interactions
Cell adhesion and interaction

Figure 5

A

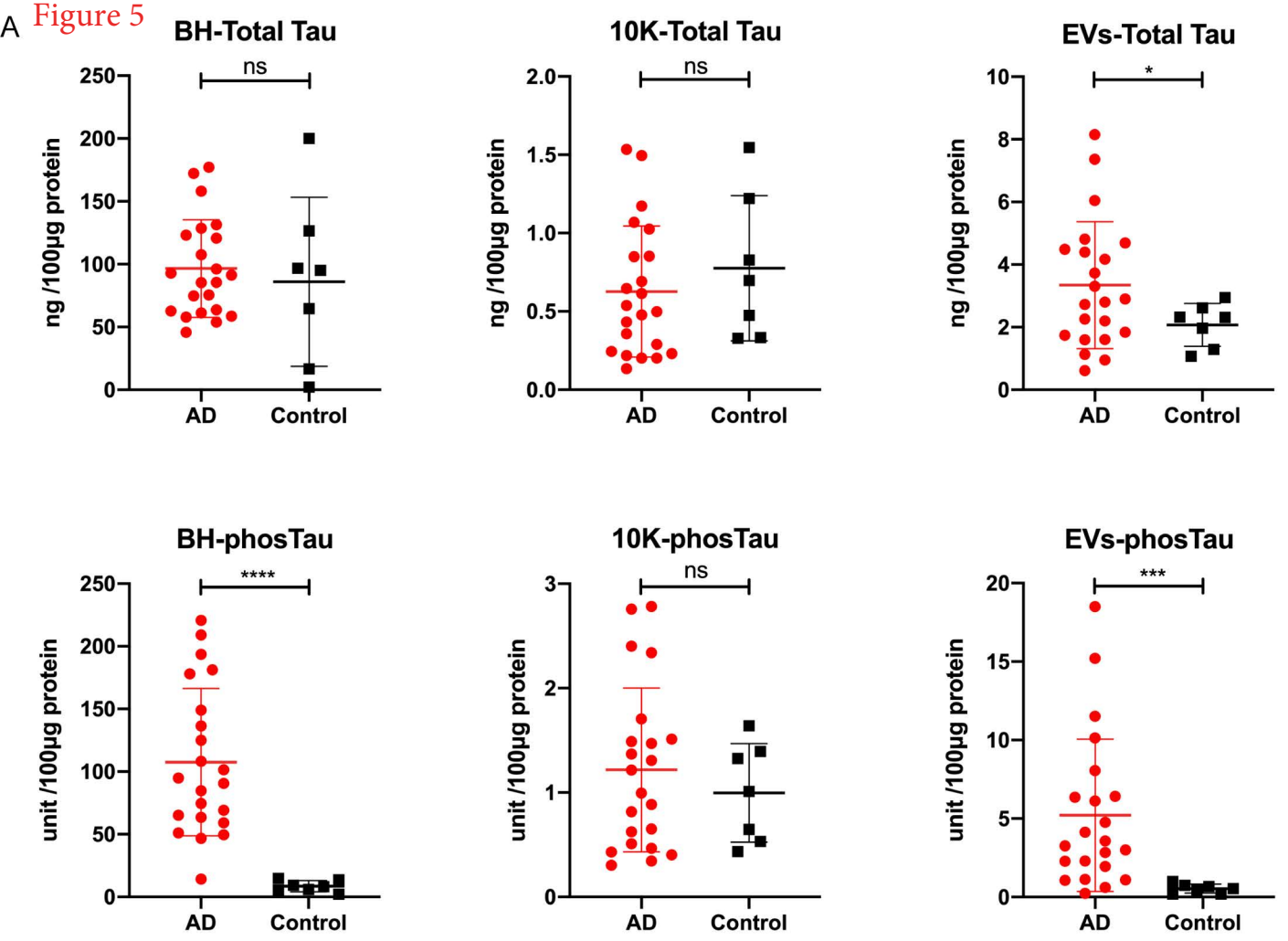
BH-Total Tau
ns
ng /100µg protein
AD
Control
10K-Total Tau
ns
ng /100µg protein
AD
Control
EVs-Total Tau
*
ng /100µg protein
AD
Control
BH-phosTau
****
unit /100µg protein
AD
Control
10K-phosTau
ns
unit /100µg protein
AD
Control
EVs-phosTau
***
unit /100µg protein
AD
Control

B

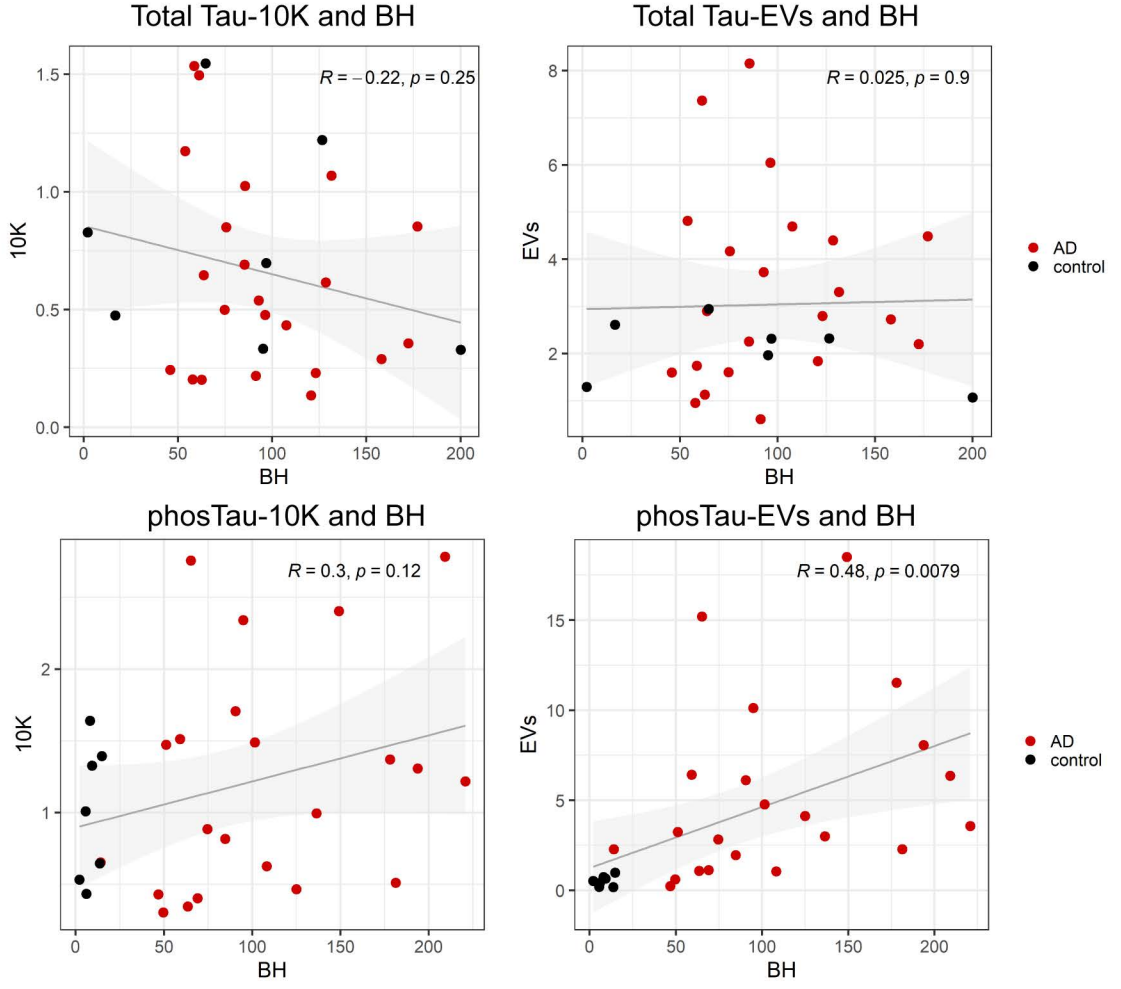
Total Tau-10K and BH
R = −0.22, p = 0.25
10K
BH
Total Tau-EVs and BH
R = 0.025, p = 0.9
EVs
BH
AD
control
phosTau-10K and BH
R = 0.3, p = 0.12
10K
BH
phosTau-EVs and BH
R = 0.48, p = 0.0079
EVs
BH
AD
control

Figure 6

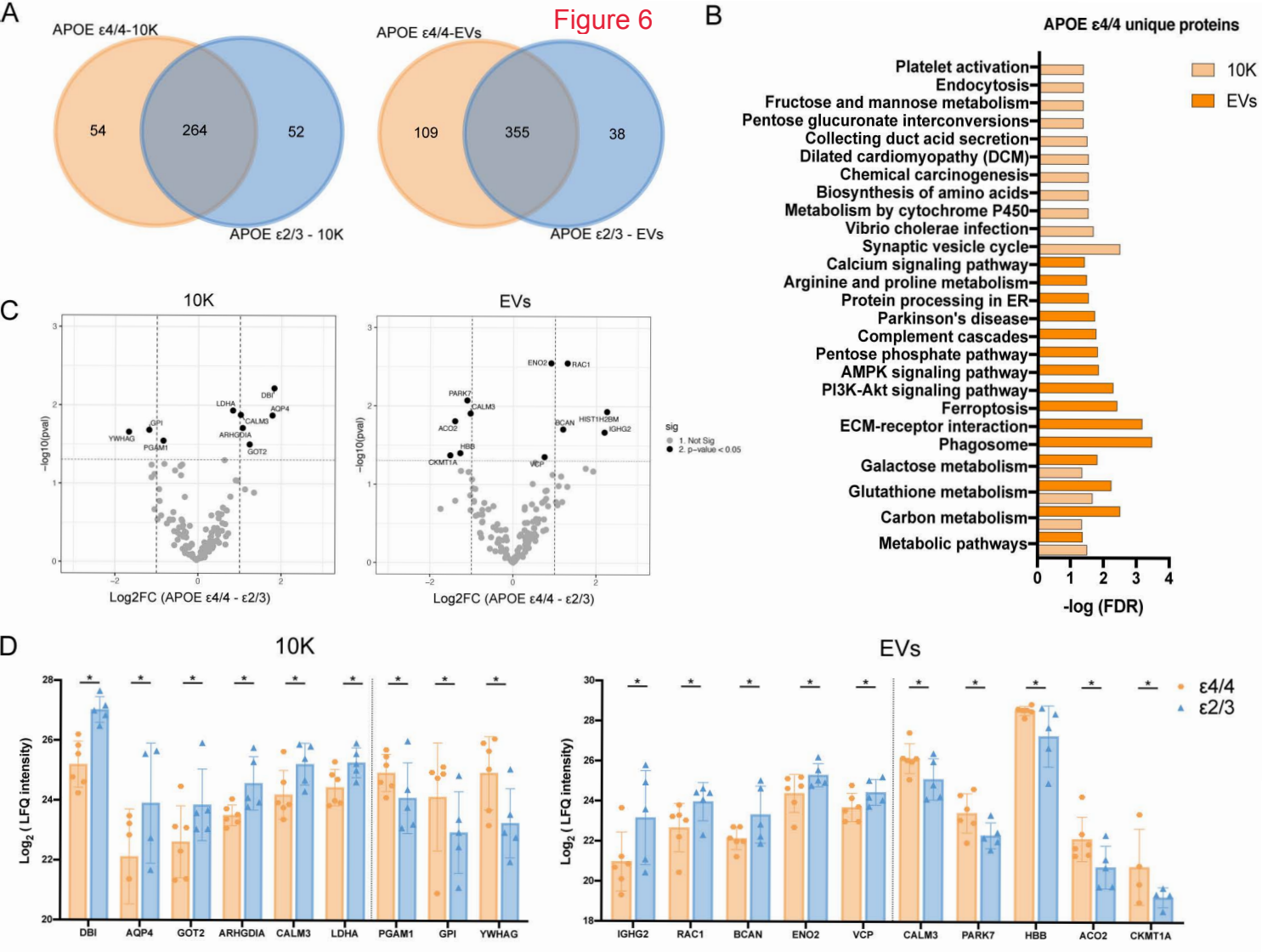
A
APOE ε4/4-10K
54
264
52
APOE ε2/3 - 10K
APOE ε4/4-EVs
109
355
38
APOE ε2/3 - EVs
B
APOE ε4/4 unique proteins
10K
EVs
Platelet activation
Endocytosis
Fructose and mannose metabolism
Pentose glucuronate interconversions
Collecting duct acid secretion
Dilated cardiomyopathy (DCM)
Chemical carcinogenesis
Biosynthesis of amino acids
Metabolism by cytochrome P450
Vibrio cholerae infection
Synaptic vesicle cycle
Calcium signaling pathway
Arginine and proline metabolism
Protein processing in ER
Parkinson's disease
Complement cascades
Pentose phosphate pathway
AMPK signaling pathway
PI3K-Akt signaling pathway
Ferroptosis
ECM-receptor interaction
Phagosome
Galactose metabolism
Glutathione metabolism
Carbon metabolism
Metabolic pathways
-log (FDR)
C
10K
EVs
-log10(pval)
Log2FC (APOE ε4/4 - ε2/3)
DBI
AQP4
LDHA
CALM3
GPI
YWHAG
ARHGDIA
PGAM1
GOT2
ENO2
RAC1
PARK7
ACO2
HBB
CKMT1A
BCAN
HIST1H2BM
IGHG2
VCP
sig
1. Not Sig
2. p-value < 0.05
D
10K
EVs
Log2 ( LFQ intensity)
DBI
AQP4
GOT2
ARHGDIA
CALM3
LDHA
PGAM1
GPI
YWHAG
IGHG2
RAC1
BCAN
ENO2
VCP
CALM3
PARK7
HBB
ACO2
CKMT1A
ε4/4
ε2/3

A Figure S1

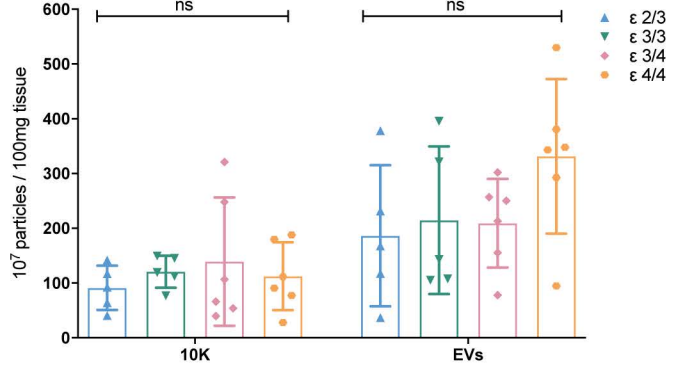
ns
ns
ε 2/3
ε 3/3
ε 3/4
ε 4/4
$10^7$ particles / 100mg tissue
600
500
400
300
200
100
0
10K
EVs

B

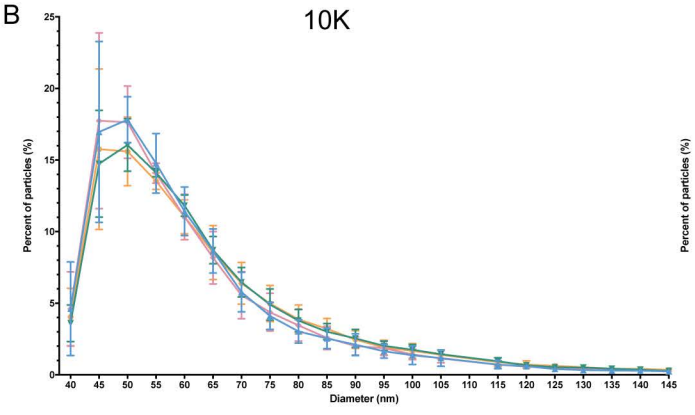
10K
Percent of particles (%)
Diameter (nm)

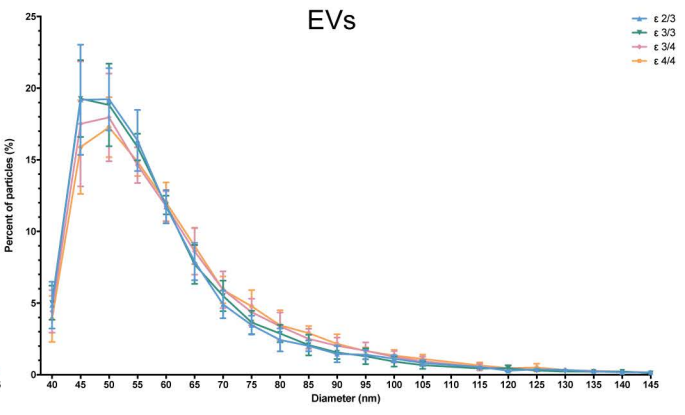
EVs
ε 2/3
ε 3/3
ε 3/4
ε 4/4
Percent of particles (%)
Diameter (nm)

Figure S2

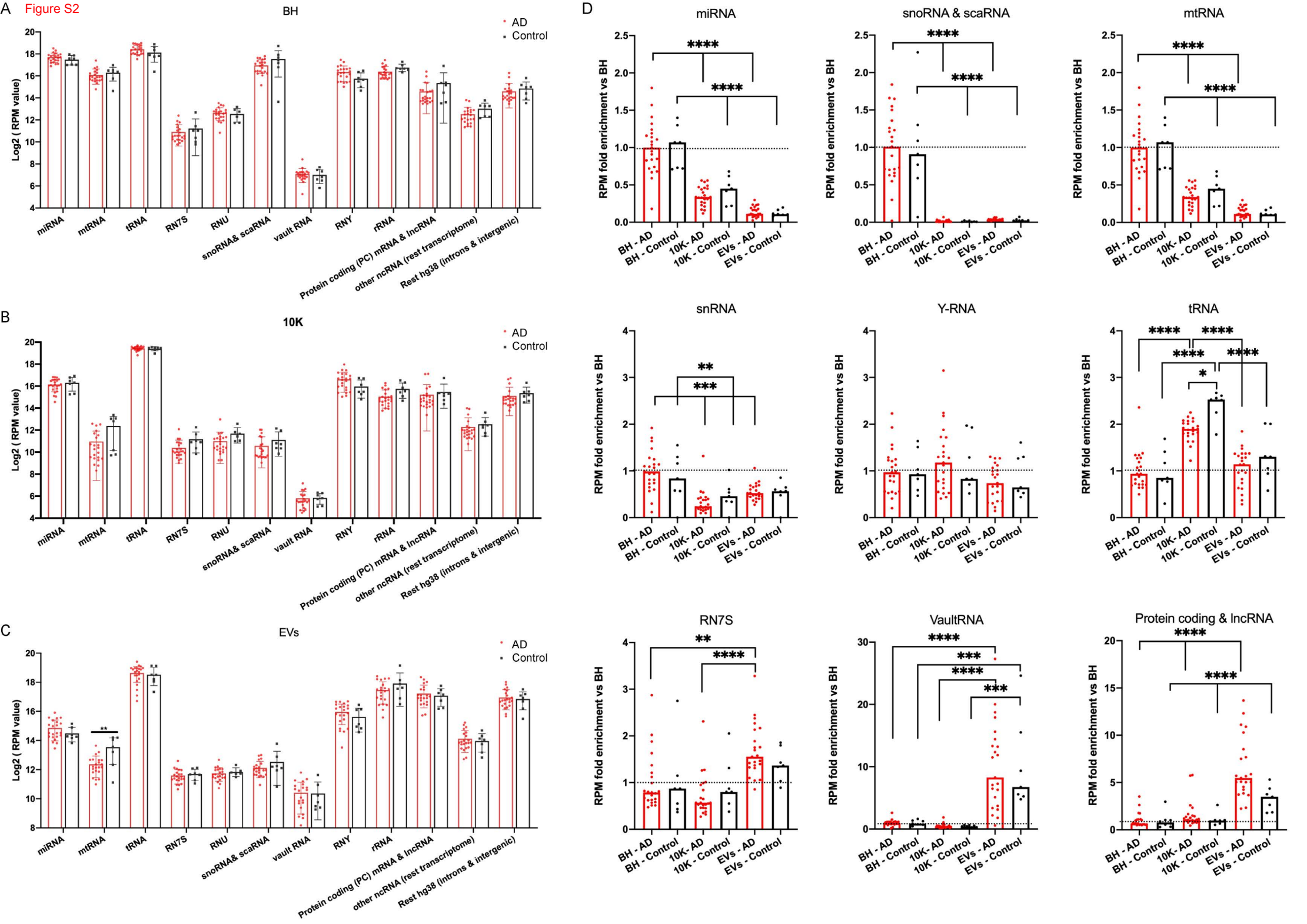
A
BH
AD
Control
Log2 ( RPM value)
miRNA
mtRNA
tRNA
RN7S
RNU
snoRNA& scaRNA
vault RNA
RNY
rRNA
Protein coding (PC) mRNA & lncRNA
other ncRNA (rest transcriptome)
Rest hg38 (introns & intergenic)
B
10K
C
EVs
D
miRNA
snoRNA & scaRNA
mtRNA
snRNA
Y-RNA
tRNA
RN7S
VaultRNA
Protein coding & lncRNA
RPM fold enrichment vs BH
BH - AD
BH - Control
10K- AD
10K - Control
EVs - AD
EVs - Control

Figure S3

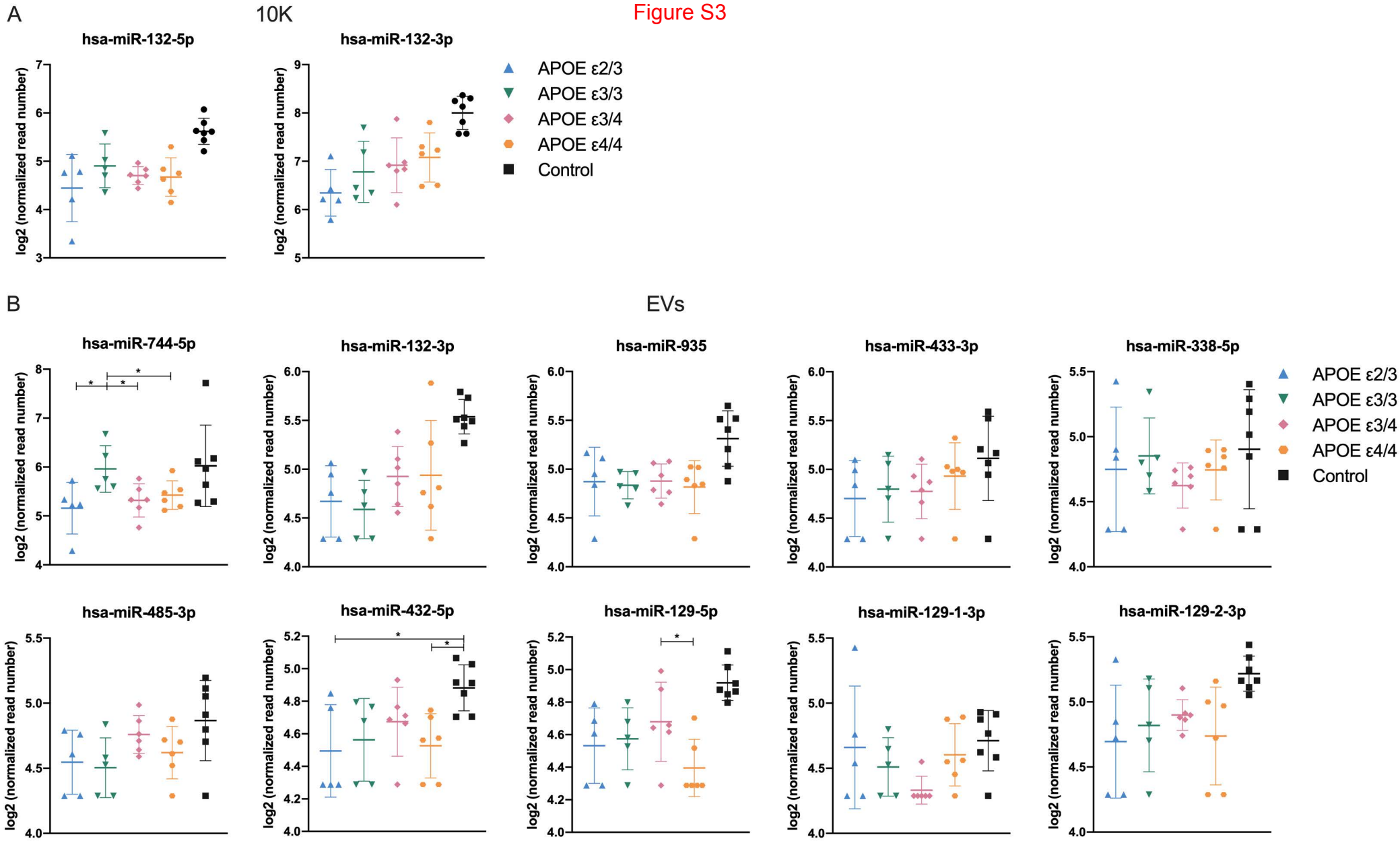
A
10K
hsa-miR-132-5p
hsa-miR-132-3p
log2 (normalized read number)
APOE ε2/3
APOE ε3/3
APOE ε3/4
APOE ε4/4
Control
B
EVs
hsa-miR-744-5p
hsa-miR-132-3p
hsa-miR-935
hsa-miR-433-3p
hsa-miR-338-5p
hsa-miR-485-3p
hsa-miR-432-5p
hsa-miR-129-5p
hsa-miR-129-1-3p
hsa-miR-129-2-3p

Figure S4

A

10K

hsa-miR-1225-5p

hsa-miR-629-5p

hsa-miR-483-5p

hsa-miR-590-5p

hsa-miR-487a-5p

hsa-miR-29b-2-5p

hsa-miR-410-3p

hsa-let-7f-2-3p

hsa-miR-23b-5p

log2 (normalized read number)

APOE ε2/3

APOE ε3/3

APOE ε3/4

APOE ε4/4

B

EVs

hsa-miR-199a-5p

hsa-miR-379-5p

log2 (normalized read number)

APOE ε2/3

APOE ε3/3

APOE ε3/4

APOE ε4/4

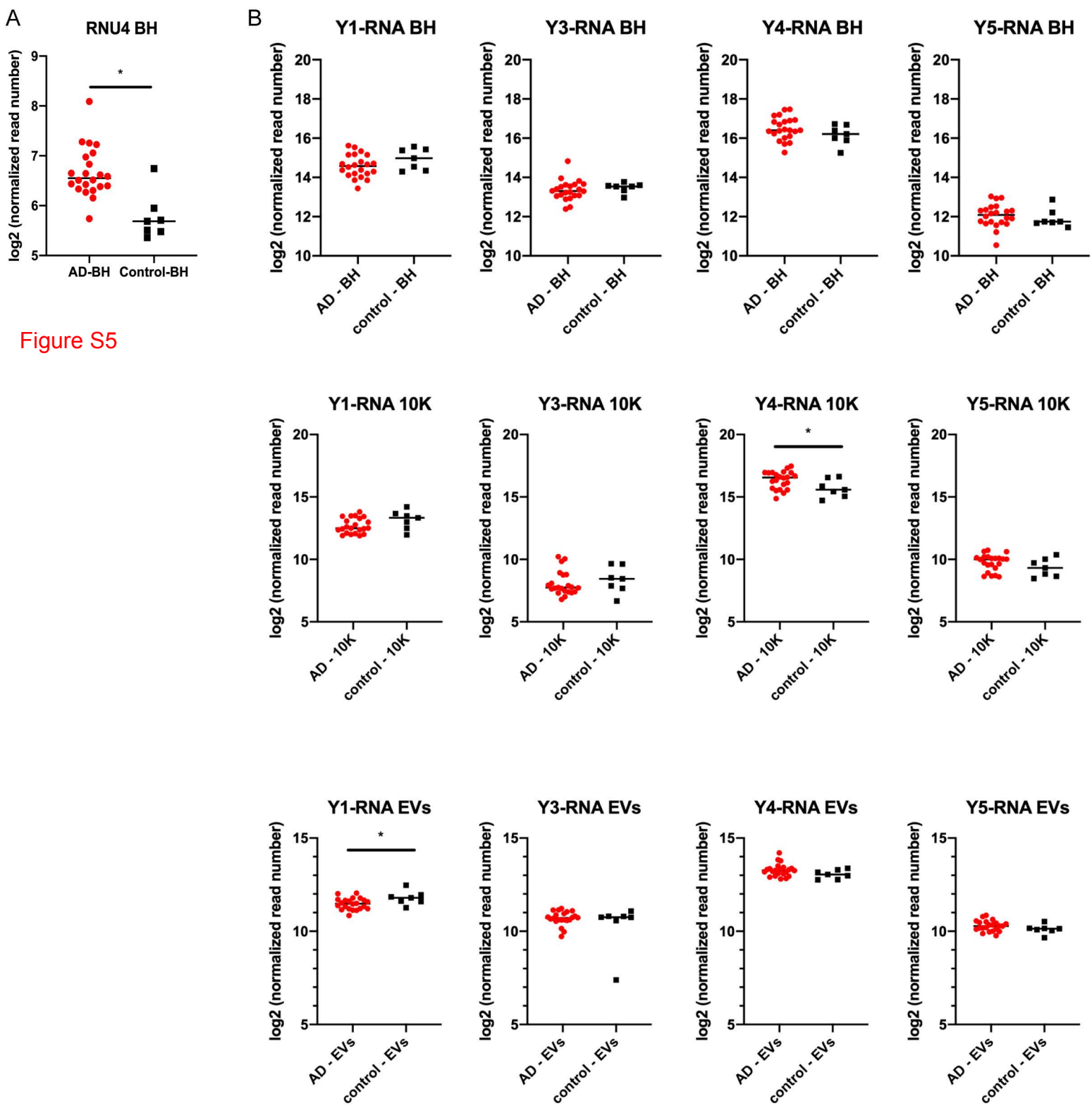
A
RNU4 BH
log2 (normalized read number)
AD-BH
Control-BH
B
Y1-RNA BH
Y3-RNA BH
Y4-RNA BH
Y5-RNA BH
AD - BH
control - BH
Y1-RNA 10K
Y3-RNA 10K
Y4-RNA 10K
Y5-RNA 10K
AD - 10K
control - 10K
Y1-RNA EVs
Y3-RNA EVs
Y4-RNA EVs
Y5-RNA EVs
AD - EVs
control - EVs

Figure S5

Figure S6

A

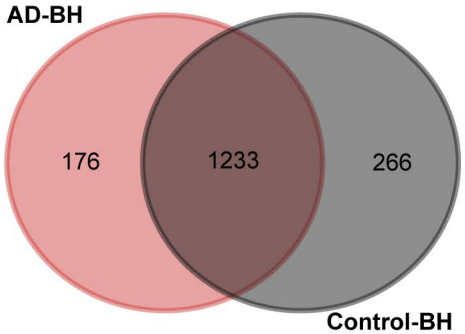


C

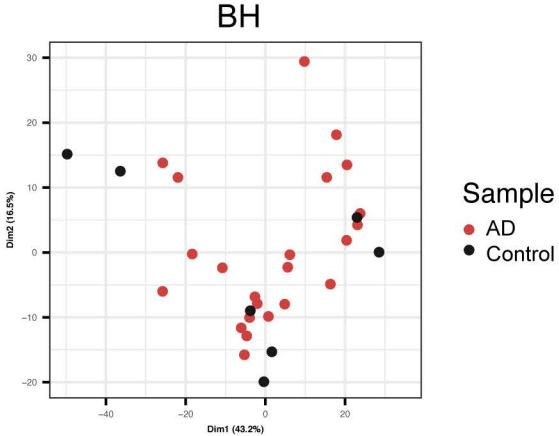


D

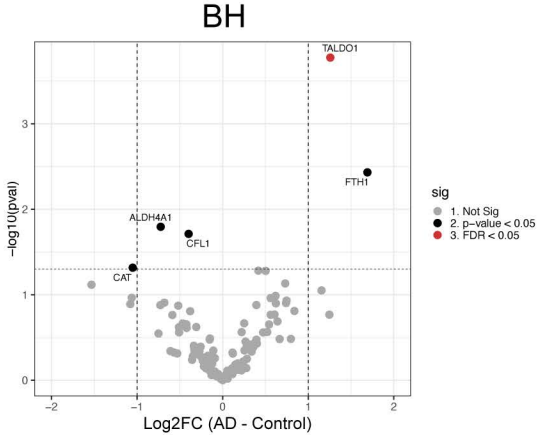


B

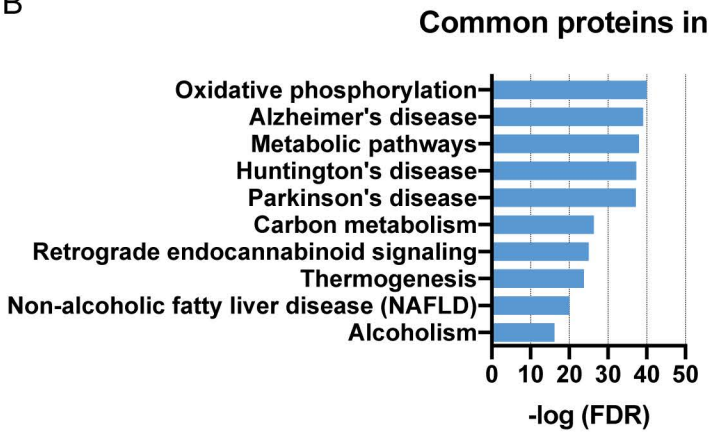


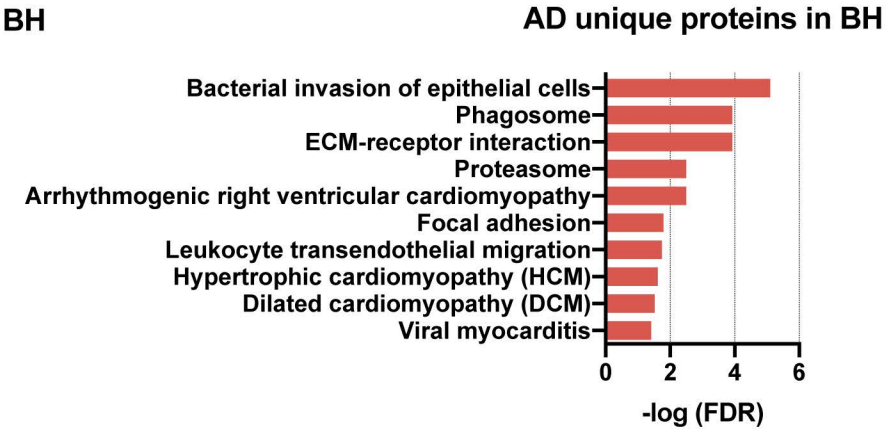

A Figure S7

10K

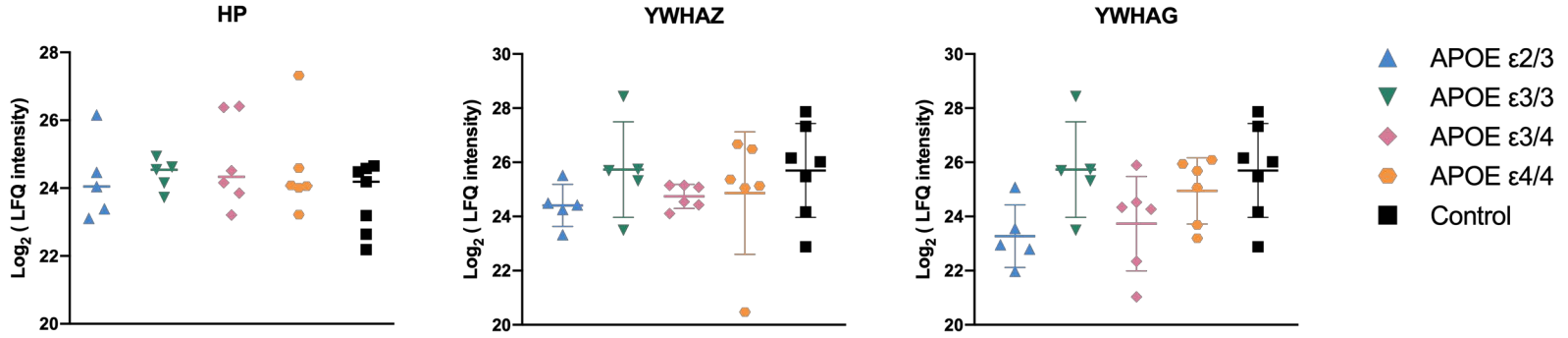


B

EVs

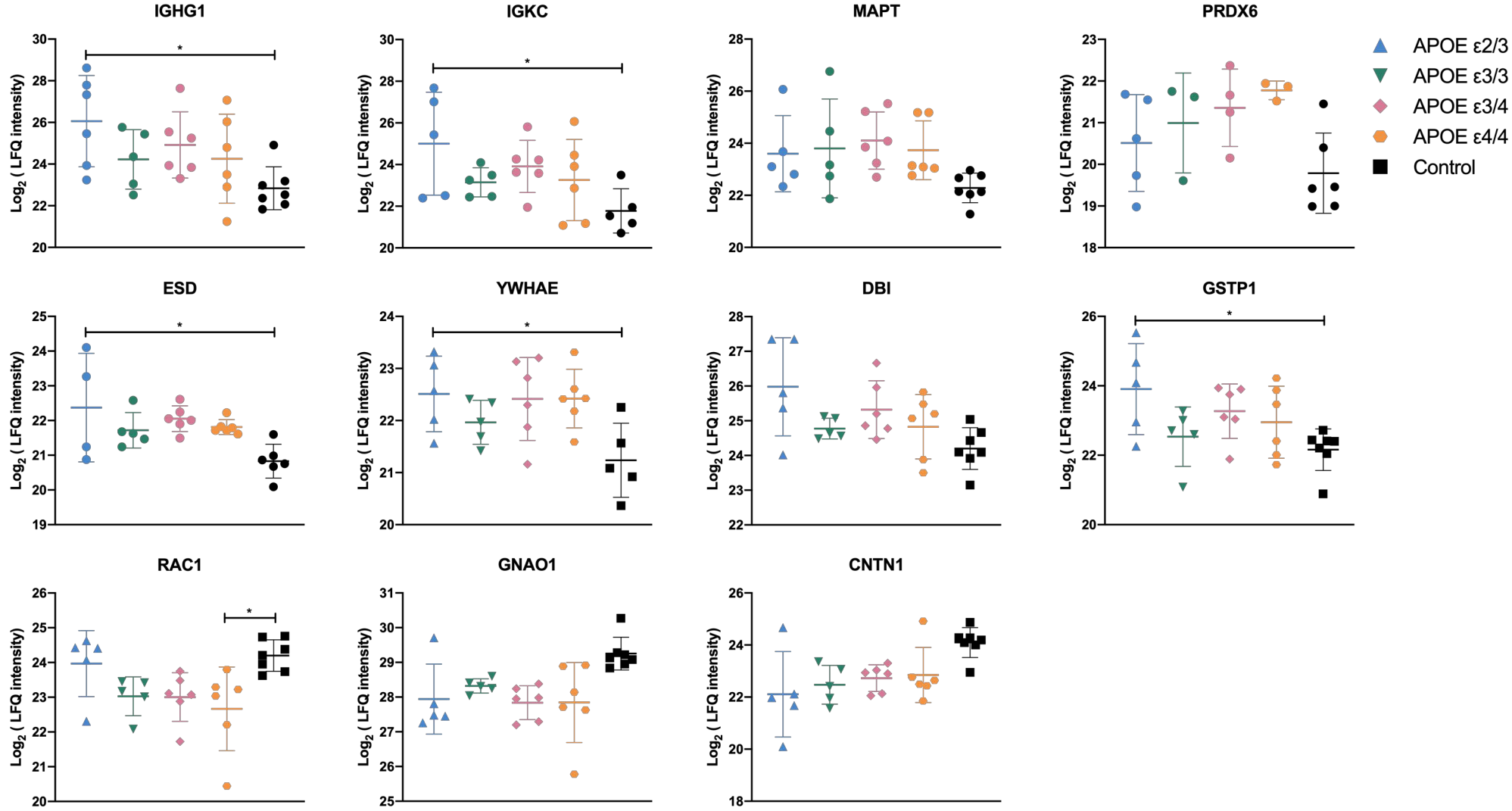

Figure S8

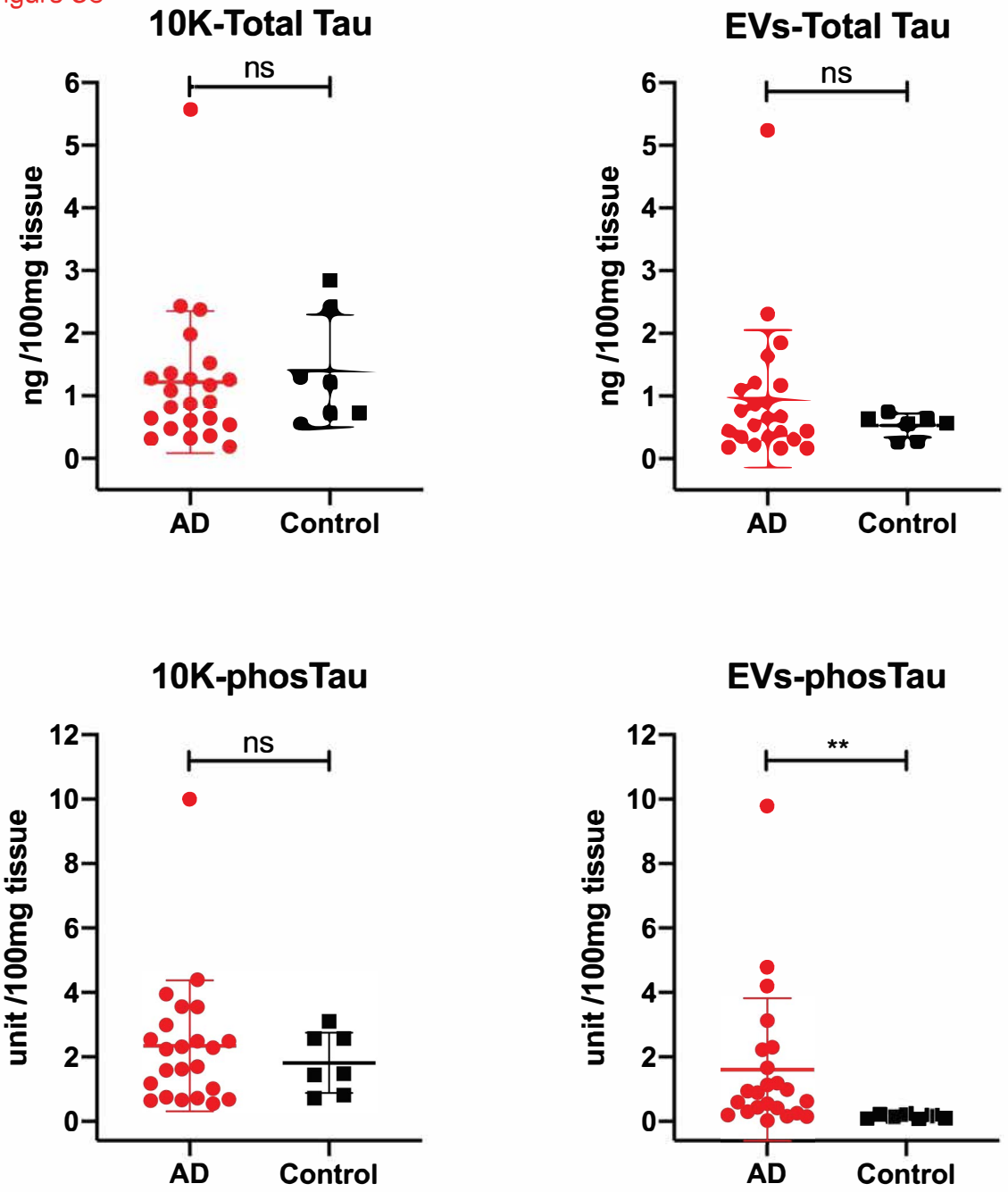
10K-Total Tau
ns
ng /100mg tissue
0
1
2
3
4
5
6
AD
Control
EVs-Total Tau
ns
ng /100mg tissue
0
1
2
3
4
5
6
AD
Control
10K-phosTau
ns
unit /100mg tissue
0
2
4
6
8
10
12
AD
Control
EVs-phosTau
**
unit /100mg tissue
0
2
4
6
8
10
12
AD
Control

Figure S9

A

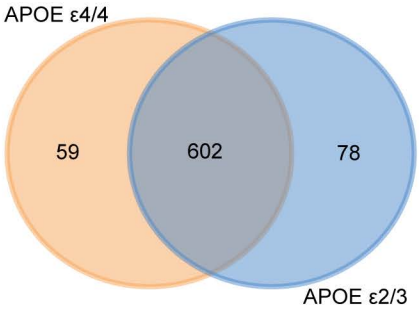


B

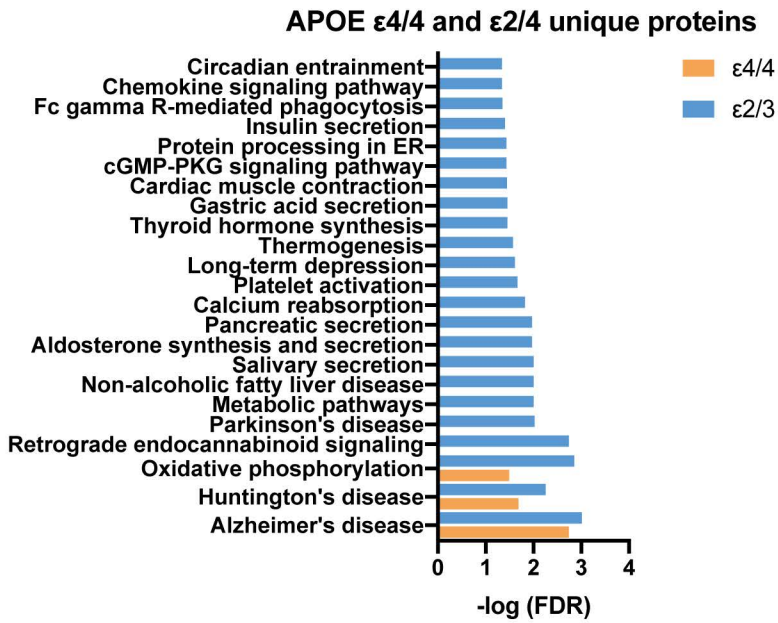


C

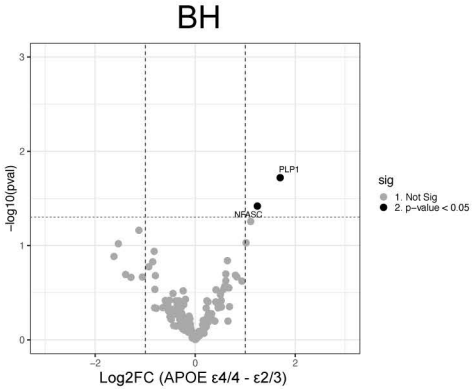

A Figure S10

10K

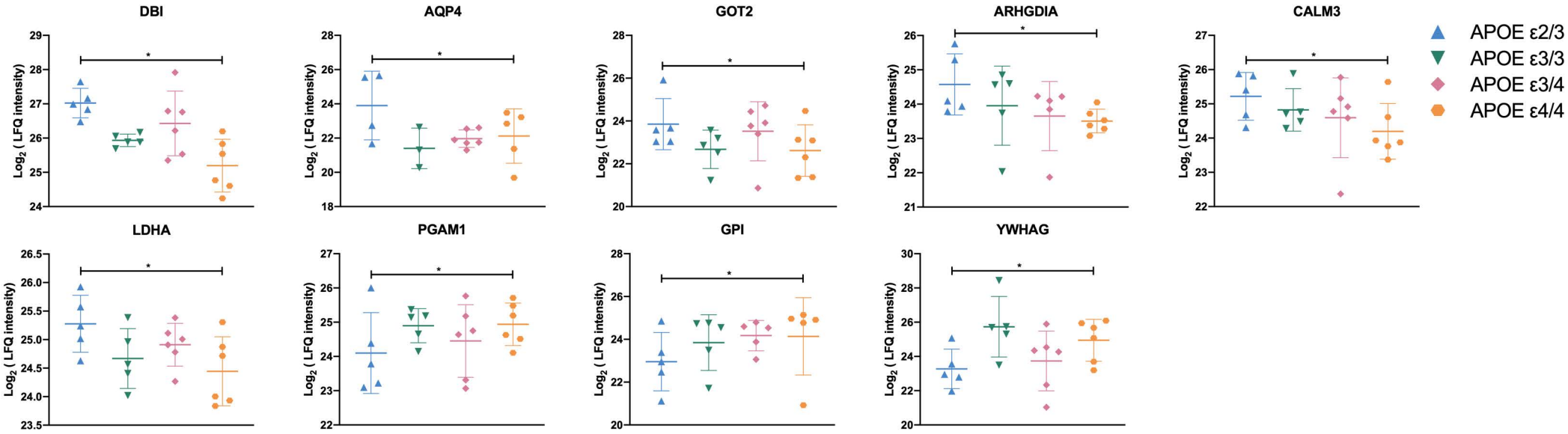


B

EVs

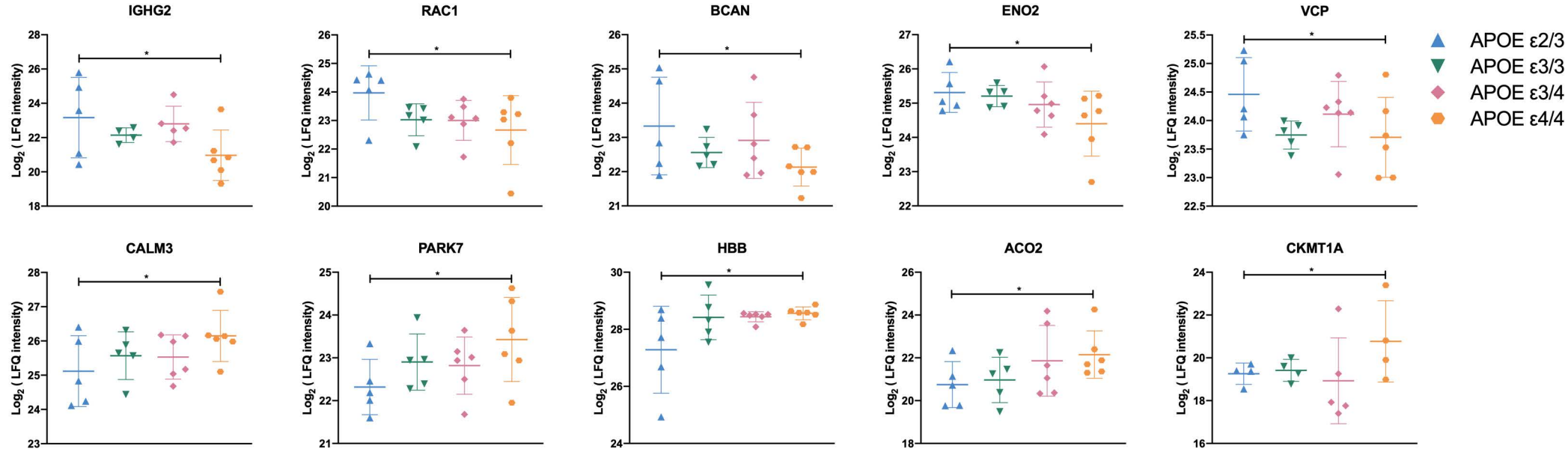

**Table 1**. Human cortex tissues used in this study

| Diag-nosis | APOE genotype | Age | Sex | RACE | Braak Stage | CERAD stage | PMI (h) |
|---|---|---|---|---|---|---|---|
| AD | E2/3 | 60s | M | W | 6 | C | 4 |
| AD | E2/3 | 60s | F | W | 6 | C | 11 |
| AD | E2/3 | 60s | M | W | 6 | C | 11 |
| AD | E2/3 | 80s | M | W | 5 | C | 5 |
| AD | E2/3 | 60s | M | W | 6 | C | 4 |
| AD | E3/3 | 80s | M | W | 6 | C | 7 |
| AD | E3/3 | 100s | F | W | 6 | B | 14 |
| AD | E3/3 | 80s | F | W | 6 | C | 8 |
| AD | E3/3 | 60s | M | W | 6 | C | 18 |
| AD | E3/3 | 80s | F | W | 6 | C | 17 |
| AD | E3/4 | 50s | F | W | 6 | C | 19 |
| AD | E3/4 | 90s | F | W | 6 | C | 21 |
| AD | E3/4 | 80s | F | W | 6 | C | 5 |
| AD | E3/4 | 80s | M | W | 6 | C | 9.5 |
| AD | E3/4 | 60s | F | W | 6 | C | 5.5 |
| AD | E3/4 | 80s | M | W | 6 | C | 18 |
| AD | E4/4 | 60s | M | W | / | / | 20 |
| AD | E4/4 | 90s | F | W | / | / | 6 |
| AD | E4/4 | 70s | F | W | / | / | 6 |
| AD | E4/4 | 90s | F | W | 6 | C | 6 |
| AD | E4/4 | 60s | F | W | / | / | 12 |
| AD | E4/4 | 70s | F | W | 6 | C | 13 |
| AD | / | 70s | M | W | 5 | C | 9 |
| Control | / | 80s | M | B | / | / | 10 |
| Control | / | 80s | M | W | / | / | 6 |
| Control | / | 50s | F | W | / | / | 6 |
| Control | E3/3 | 70s | M | W | 2 | / | 4 |
| Control | / | 90s | F | W | 1 | / | 8 |
| Control | / | 80s | F | W | 2 | / | 7 |
| Control | / | 90s | M | W | 2 | / | 15 |

Sex: M = male; F = female; Race: W = White; B = Black or African American; PMI: post-mortem interval

**Table 2**. Significantly different miRNAs (adjust P value < 0.05) with at least twofold change between AD and control in EVs and 10K. Up/downregulation of these EV miRNAs was compared with brain miRNA change in three earlier studies. Studies that have identified involvement of these miRNAs in AD are listed, as well as the potential target genes of the miRNAs.

| EV type | miRNA | Log (RPM) | Log2FC (AD/ CTRL) | P-adj | Cogswell 2008 (18525125) | Lau 2013 (24014289) | Wang 2011 (20936480) | mRNA target in literature (PMID) |
|---|---|---|---|---|---|---|---|---|
| EVs | miR-132-3p | 7.73 | -2.079 | 1.56E-03 | down | down | - | Targets effectors of abnormal Tau phosphorylation GSK-3beta and Calcineurin/PP2B, impairs Tau metabolism (26362250) MiR-132 deficiency affects MeCP2 in cortex BDNF in hippocampus, miR-132 deficiency affects memory formation and retention (25813747) MiR-132 regulates dendritic growth and arborization of neurons (MiR-132 regulates dendritic growth and arborization of neurons (21059906) |
| | miR-935 | 6.24 | -1.354 | 5.55E-03 | - | - | - | Role in AD unclear |
| | miR-433-3p | 5.31 | -1.273 | 2.15E-02 | - | down | - | Targets FGF20, which affects alpha-syn levels in Parkinson's disease (18252210) |
| | miR-129-2-3p | 5.28 | -1.241 | 2.15E-02 | - | down | down | Targets FMR1, involved in learning, memory and autistic behavior (23390134) |
| | miR-129-1-3p | 1.17 | -2.154 | 2.49E-02 | - | - | - | - |
| | miR-129-5p | 1.95 | -1.826 | 2.49E-02 | - | down | down | Targets SOX6 which protects from apoptosis / neuroinflammation (31564203) |
| | miR-338-5p | 2.40 | -1.481 | 3.12E-02 | down | - | down | Targets BACE1 (30576233) |
| | miR-338-5p | 3.20 | -1.515 | 4.37E-02 | down | - | down | Targets mitochondrial COXIV, a protein involved in oxidative phosphorylation in neurons (19020050) |
| | miR-744-5p | 26.42 | -1.375 | 4.96E-02 | - | up | - | Targets NPAS4, protein involved in neuronal differentiation and which affects BDNF (27189618) |
| | miR-432-5p | 2.00 | -1.329 | 4.96E-02 | - | - | down | Targets Suppressor of Cytokine Signaling 5 (SOCS5), link with neuroinflammation ( 27282499) |
| | miR-485-3p | 2.40 | -1.481 | 3.12E-02 | - | down | down | Targets BACE1 and is counteracted by lncRNA BACE1 antisense (20507594) |
| 10K | miR-132-5p | 17.15 | -1.249 | 1.76E-06 | down | down | - | see miR-132 in EVs |
| | miR-132-3p | 145.42 | -1.020 | 2.19E-04 | down | down | - | see miR-132 in EVs |

P-adj: adjusted P value.

**Table 3**. Significantly different miRNAs (adjusted P value < 0.05) with twofold change between APOE ε4/4 and ε2/3 carrier in EVs and 10K. Up/downregulation of these EV miRNAs was compared with brain miRNA change in three earlier studies. Studies that have identified involvement of these miRNAs in AD are listed, as well as potential target genes of the miRNAs.

| EV type | miRNA | logRPM | Log2FC (APOE ε4/4 / APOE ε2/3) | p-value | Previously reported mRNA targets (PMID) |
|---|---|---|---|---|---|
| EV | miR-199a-5p | 3.21 | 1.275 | 1.71E-02 | targets ApoE in melanoma (23142051), targets CD44 in cancer (22498306), CD44 KO mice have spatial memory deficits (25219362) |
| | miR-379-5p | 1.70 | -1.093 | 2.16E-02 | deletion of miR-379 in mice causes anxiety behavior (26744330), AD patients can have increased anxiety |
| 10K | miR-483-5p | 29.70 | 1.819 | 2.96E-03 | targets epigenetic regulator methyl CpG-binding protein 2 (MeCP2) (23431031) |
| | miR-29b-2-5p | 9.33 | -1.208 | 5.90E-03 | targets BACE1 which is involved in Abeta formation (18434550) |
| | miR-23b-5p | 2.76 | -2.622 | 9.72E-03 | downregulation of miR-23a in brain injury causes neuronal cell loss (25057207) |
| | miR-487a-5p | 9.33 | -1.120 | 1.09E-02 | downregulated in AD (20936480, 24014289) |
| | miR-410-3p | 5.96 | -1.263 | 1.55E-02 | deletion of miR-410 in mice causes anxiety behaviour (26744330), AD patients can have increased anxiety |
| | let-7f-2-3p | 5.28 | -1.403 | 1.66E-02 | unclear |
| | miR-629-5p | 1.44 | 2.788 | 2.22E-02 | unclear |
| | miR-590-5p | 6.90 | 1.249 | 3.33E-02 | unclear |
| | miR-1225-5p | 1.27 | 3.091 | 3.53E-02 | unclear |

**Table 4.** The potential function of significantly different proteins (P value < 0.05) between APOE ε4/4 and ε2/3 carriers in EVs

| Protein symbol | Protein name | Enriched in | Functions | Reference (PMID) |
|---|---|---|---|---|
| RAC1 | Ras-related C3 botulinum toxin substrate 1 | ε 2/3 | Rho-GTPases, membrane remodeling | 30594931, 30005699, 29330095 |
| BCAN | Brevican core protein | ε 2/3 | neurite outgrowth, stabilizes synapses | 11015614, 2132834 |
| ENO2 | γ-enolase | ε 2/3 | neurotrophic and neuroprotective | 23621429, 7753500, 22257123 |
| VCP | Transitional endoplasmic reticulum ATPase | ε 2/3 | mitochondrial mitophagy impairment, abnormal protein aggregate and clearance | 27561680, https://doi.org/10.1016/j.bbamcr.2011.07.001 |
| CALM3 | Calmodulin-3 | ε 4/4 | cytosolic Ca2+ concentration regulation | 9237482 |
| PARK7 | Protein deglycase DJ-1 | ε 4/4 | antioxidant defense | 16517609, 26907355 |
| ACO2 | Aconitate hydratase | ε 4/4 | energy metabolism, mitochondrial function | 13894501, 13894501 |
| CKMT1A | Creatine kinase U-type | ε 4/4 | ATP production | 20639122, 26907355 |
| HBB | Hemoglobin subunit beta | ε 4/4 | oxygen homeostasis regulation | 19116637, 24333691 |

**Table 5.** The potential function of significantly different proteins (P value < 0.05) between APOE ε4/4 and ε2/3 carrier in 10K

| Protein symbol | Protein name | Enriched in | Function in CNS disease | Reference (PMID) |
|---|---|---|---|---|
| DBI | Acyl-CoA-Binding Protein | ε 2/3 | GABA receptor modulation; neurogenesis | 1664069, 22226357, 28343864 |
| GOT2 | Glutamate oxaloacetate transaminase, mitochondrial | ε 2/3 | mitochondrial energy metabolism | 23600763 |
| ARHGDIA | Rho GDP-dissociation inhibitor 1 | ε 2/3 | modulation of GTPases; cell motility regulation | 27841340 |
| CALM3 | Calmodulin-3 | ε 2/3 | cytosolic Ca2+ concentration regulation | 9237482 |
| LDHA | L-lactate dehydrogenase A chain | ε 2/3 | glycolysis | 31112527 |
| PGAM1 | Phosphoglycerate mutase 1 | ε 4/4 | glycolysis metabolism; cell proliferation; | 27572934, 30460638 |
| GPI | Glucose-6-phosphate isomerase | ε 4/4 | glycolysis metabolism; neuroleukin function | 29905912, 28803808, 3352745 |
| YWHAG | 14-3-3 protein gamma | ε 4/4 | neuronal differentiation | 29075177, 30853823 |

**Supplemental Table 1**. Number of proteins identified in each type of sample/fraction

| Groups | BH | 10K | EVs |
|---|---|---|---|
| All samples | 1675 | 801 | 1197 |
| Control | 1399 | 530 | 847 |
| AD | 1329 | 728 | 1047 |